

Analytic evolution for complex coupled tight-binding models: Applications to quantum light manipulation

Santiago Rojas-Rojas ^{1,2,*}, Camila Muñoz,^{1,3} Edgar Barriga,⁴ Pablo Solano,^{1,5}
Aldo Delgado ^{1,2} and Carla Hermann-Avigliano^{2,3}

¹*Departamento de Física, Facultad de Ciencias Físicas y Matemáticas, Universidad de Concepción, Concepción, Chile*

²*Millennium Institute for Research in Optics (MIRO), Chile*

³*Departamento de Física, Facultad de Ciencias Físicas y Matemáticas, Universidad de Chile, Santiago, Chile*

⁴*Departamento de Física, Facultad de Ciencias, Universidad de Chile, Santiago, Chile*

⁵*CIFAR Azrieli Global Scholars program, CIFAR, Toronto, Canada*



(Received 21 November 2023; accepted 8 July 2024; published 27 August 2024)

We present analytic solutions to the evolution in generalized tight-binding models, which consider complex first-neighbor couplings with equal amplitude and arbitrary phases. Our findings provide a powerful tool to efficiently calculate expectation values and correlations within the system, which are otherwise difficult to compute numerically. We apply our results to relevant examples in quantum light manipulation using N -port linear couplers, describing the evolution of single (multi)-mode squeezing, single-photon added (subtracted) Gaussian states, and second-order site-to-site photon correlations. Significantly, our analytic results outperform standard numerical calculations. Our study paves the way for a comprehensive mathematical framework describing the spatial evolution of quantum states across a wide range of physical systems governed by the tight-binding model.

DOI: [10.1103/PhysRevResearch.6.033224](https://doi.org/10.1103/PhysRevResearch.6.033224)

I. INTRODUCTION

A good physical model captures the nature of a phenomenon through a simple mathematical description; however, simple descriptions do not always lead to simple solutions. The tight-binding (TB) model is an iconic example of this. Noninteracting particles hopping between adjacent sites describe the essence of the quantum behavior of electrons in solids, their transport properties, and band structure. Although initially intended to describe electrons in solids [1], the TB model characterizes analogous systems such as optical lattices with cold atoms [2–4], light propagating in lattice waveguides [5–8], phononic crystals [9], surface waves and topological insulators [10–12], and quantum random walks [13,14]. Regardless of the simplicity of the TB model, many configurations lack analytic solutions in real space, and standard approaches resort to solving the problem in momentum space or through numerical methods. These approaches, however, pose a challenge for modeling the dynamics of spatial distributions and correlations of particles—critical aspects of quantum systems.

Although the TB model in the second quantization formalism describes a linear evolution, its Hilbert space dimension grows exponentially with the number of sites, presenting

a significant computational problem [14]. For example, the seemingly simple scenario of a TB model with linear coupling between arbitrary sites lacks a real-space analytic solution to efficiently compute transport and correlations dynamics. Even approximated numerical methods with a truncated Hilbert space, mean-field descriptions [2], or solving for the ground state [15] are resource-intensive tasks for classical computers [16]. More importantly, quantum phenomena generally arise from correlations beyond the mean field, while correlations between particles across lattice sites are not captured in the momentum-space representation that diagonalizes the TB Hamiltonian. Thus, we need techniques beyond the standard ones to calculate the real-space evolution of many-body quantum systems.

The previous limitations are especially relevant for multimode quantum light engineering, where correlations are crucial. For example, an N -port linear coupler described by a TB model can be used to produce multimode squeezed states [17], besides the multiple applications it has for technologies based on integrated photonics [18]. Furthermore, states generated by the addition or subtraction of photons on Gaussian states find an extension to multimode systems, producing a plethora of nonclassical states such as two-mode photon-added entangled coherent squeezed states [19], (superpositions of) photon-added trio-coherent states [20], and photon-added and photon-subtracted four-mode squeezed vacuum states [19,21]. Multimode quantum optics find applications in quantum technologies such as information processing [22], metrology [23–25], and cryptography [26], evidencing the relevance of calculating the evolution and the correlations of such states. Although real coupling coefficients describe the interactions in the above examples,

*Contact author: santirojas@udec.cl

Published by the American Physical Society under the terms of the [Creative Commons Attribution 4.0 International](https://creativecommons.org/licenses/by/4.0/) license. Further distribution of this work must maintain attribution to the author(s) and the published article's title, journal citation, and DOI.

many other models rely on complex coefficients [27–30]. For instance, complex phases of the coupling constants simulate a fictitious vector potential in honeycomb photonic lattices demonstrating photonic topological insulation [31], display an effective gauge potential for photons with synthetic dimensions in photonic lattices [32], and lead to non-Hermitian Hamiltonians describing phenomena such as Bloch oscillations, the invisibility of defects, and \mathcal{PT} -symmetric quantum fields [33].

This work presents an analytic real-space solution to the one-dimensional TB model for complex coupling constants with equal amplitudes and arbitrary phases. Our method draws upon tools from graph theory to analytically calculate all the elements of the transformation matrix for closed and open arrays, deriving expressions for the evolution of functions that depend on the annihilation and creation operators. The solution allows us to efficiently analyze transport dynamics and the propagation of spatial quantum correlations, outperforming numerical computations.

We demonstrate the advantages of our findings by addressing problems related to quantum light propagation in an arbitrary N -port array of linear couplers. First, we elucidate the generation of multimode squeezing from single-mode squeezing. Second, we explore the dynamics of single-photon added or subtracted Gaussian states, providing a precise analytical depiction of their N -mode Wigner function, extending recent results [34] to the multimode regime. Third, we provide an analytic solution for propagating second-order photon correlations through coupling phase disorder. In particular, we show that two-photon entangled states exhibit an interference term in their second-order correlation that decreases exponentially with the degree of phase disorder, transitioning from a quantum to classical behavior. Finally, we benchmark our analytic solutions against standard numerical solvers, proving their computational advantage. Our results enable the analysis of spatial evolution and correlation dynamics in an extended one-dimensional TB model with numerous particles. This approach broadens the scope of linearly coupled systems beyond traditional mean-field approximations and paves the way to explore analytical solutions in varied spatial configurations.

II. FIELD MODE TRANSFORMATIONS IN AN N -DIMENSIONAL COUPLER

We consider a system of N coupled bosonic modes described by the Hamiltonian

$$H = \hbar \sum_{(j,k)} (C_{jk} a_j^\dagger a_k + C_{jk}^* a_k^\dagger a_j), \quad (1)$$

where a_j (a_j^\dagger) is the annihilation (creation) operator of an excitation in the j th mode. In the most general case, the sum runs over all the ordered pairs of modes, whose coupling is determined by the respective complex coefficient C_{jk} . In the context of the examples given in this work, this Hamiltonian describes a linear device with $N \times N$ input-output ports. We interchangeably refer to the system as a coupler, array, or N -mer.

We use a Heisenberg picture approach for N -bosonic modes and apply it to the open and closed TB model with

complex coupling coefficients (see Fig. 1). The evolution of each mode is computed as a transformation of the bosonic operators a_m into new bosonic operators a'_m , given by

$$a'_m = U^\dagger a_m U, \quad (2)$$

where $U = \exp(-iHt/\hbar)$ is the evolution operator. This input-output approach is suitable for studying the spatial evolution and correlations of arbitrary states in an N -mode system, as it is state independent.

The Baker-Campbell-Hausdorff (BCH) formula allows us to express the transformed operators a'_m as

$$a'_m = a_m + \left[\frac{i}{\hbar} t H, a_m \right] + \frac{1}{2!} \left[\frac{i}{\hbar} t H, \left[\frac{i}{\hbar} t H, a_m \right] \right] + \dots, \quad (3)$$

or, equivalently,

$$a'_m = \sum_{n=0}^{\infty} \frac{1}{n!} \left(\frac{it}{\hbar} \right)^n [H, a_m]_n, \quad (4)$$

with

$$[H, a_m]_n = [H, [H, a_m]_{n-1}] = \sum_{j=1}^N \Lambda_j^{(n)} a_j, \quad (5)$$

and $[H, a_m]_0 = a_m$. The right-hand side arises from the canonical commutation relations and implies that each term in the iterative sum in Eq. (4) is a linear combination of the N modes of the field. Substituting with the definition of H in Eq. (1), we obtain

$$\Lambda_j^{(n+1)} = -\hbar \sum_{\ell(j)} C_{\ell(j),j} \Lambda_{\ell(j)}^{(n)}, \quad (6)$$

where the sum over ℓ is restricted to the modes connected to the j th mode through the coupling constants. Thus, the set of coefficients $\Lambda_n^{(n)}$ and $\Lambda_n^{(n+1)}$ is related through the Hermitian *coupling matrix* \mathcal{C} , which corresponds to the single-particle representation of the Hamiltonian in Eq. (1). Using Eq. (6), we can write Eq. (4) as

$$a'_m = \sum_{n=0}^{\infty} \frac{1}{n!} \left(\frac{it}{\hbar} \right)^n \left[\sum_{j=1}^N \hat{e}_j^\top (-\hbar \mathcal{C}^\top)^n \hat{e}_m a_j \right], \quad (7)$$

where \hat{e}_j denotes the j th vector in the canonical basis. The information specific to the array is present in each term through the coupling matrix \mathcal{C} . Writing the modes operators as the components of vectors \vec{a}' and \vec{a} , the above expression can be written as

$$\vec{a}' = A^{(N)} \vec{a}, \quad (8)$$

where the $N \times N$ matrix $A^{(N)}$ is the exponential of the coupling matrix \mathcal{C} (see Appendix A for details), that is,

$$A^{(N)} = \exp(-it\mathcal{C}). \quad (9)$$

Thereby, determining the evolution of functions of bosonic operators depends on evaluating the transformation matrix $A^{(N)}$.

The dependence of operators a_i on the dynamical variable t provides a convenient framework to describe the evolution of specific observables, such as the mean photon number or the field quadratures [35,36] as well as classical and quantum correlations on few-particle systems [13,14]. The dynamics

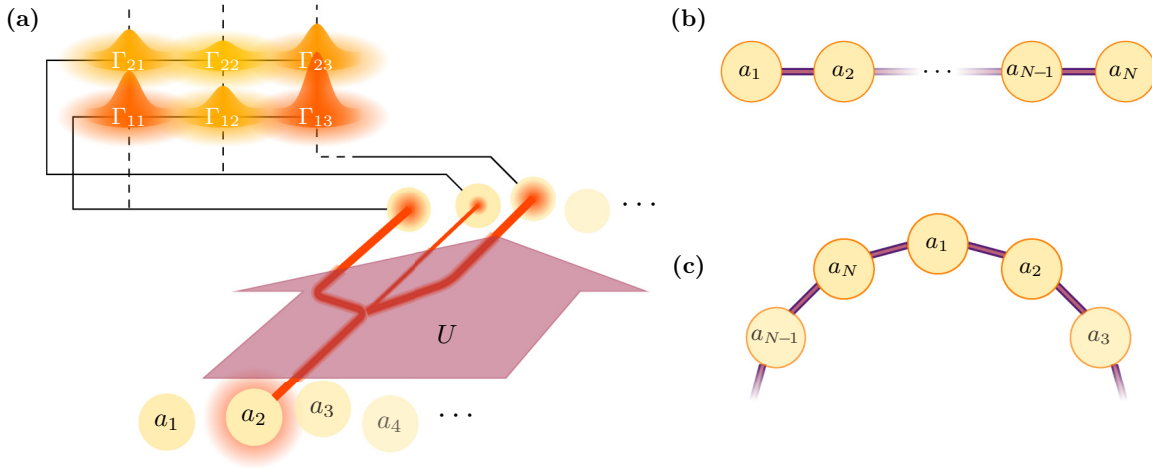


FIG. 1. (a) N -mode linear coupler. We consider a one-dimensional system sustaining N modes of a bosonic field. The system evolves according to the transformation $U = \exp(-iHt)$ associated to the Hamiltonian in Eq. (1), allowing adjacent modes to couple according to a TB model with complex coefficients C_j . After evolution, we can analytically compute different observables or correlations Γ_{ij} . (b) and (c) show a schematic of an open and closed array, respectively.

of the TB model can be studied by numerically solving the associated Schrödinger equation [37]. Considering N modes and, at most, D excitations per mode, the effective dimension of the Hilbert space is given by D^N . This exponential scaling severely limits this approach when computational resources are scarce (see the graphical representation in Ref. [14]). Given the linearity of the TB model, which conserves the total excitation number and neglects interaction between particles, it is possible to calculate the dynamics via the $N \times N$ transformation matrix $A^{(N)}$, as discussed in the above paragraphs. It can be diagonalized using several methods, such as direct diagonalization or matrix Padé approximations, which are among the most used. Unfortunately, the associated algorithms have unfavorable arithmetic complexities, which in the case of diagonalization scales as $O(N^3)$. Here, we provide methods to analytically calculate the transformation matrix $A^{(N)}$ for N arbitrary and open and closed arrays, thus avoiding computational resource limitations.

A. Approaches to determine $A^{(N)}$

The problem reduces to finding the entries $A_{m,n}^{(N)}$ of the matrix $A^{(N)}$, which are particular to the geometry defining the interacting modes, i.e., the set of pairs in the sum in Eq. (1). The first approach would be to diagonalize the Hamiltonian. However, one can only do so analytically in particular cases [35]. Other methods allow obtaining an explicit expression for the $A_{m,n}^{(N)}$, whose suitability differs for each specific coupling matrix C . For example, as discussed in Appendix C, by grouping the terms as factors of each mode a_m , the expansion in Eq. (3) indicates that each entry $A_{m,n}^{(N)}$ is, in fact, expressible as a series expansion on the amplitude of the coupling coefficients C_{jk} , whose terms follow an integer sequence. The iterative relation between successive terms can be derived from known integer sequences or a generating function [38] that is specific for each mode coupling configuration. Indeed, this approach provides an expression for the entries $A_{m,n}^{(N)}$, but translates the problem into finding the initial condition

for the respective sequence in their expansion. We find that the previous approach based on integer sequences is more convenient for studying the closed TB model with complex coupling coefficients. At the same time, direct evaluation of the exponential in Eq. (9) is advantageous for specific arrays. We present two illustrative examples in Fig. 2.

On the other hand, the coupling matrix C links to graph theory since it is the adjacency matrix of the connected graph where the propagating particles describe a quantum random walk (QRW) [13,14]. This framework relates the system to an underlying support graph [39], where each mode corresponds to a vertex while their couplings are the weighted edges. This correspondence includes the case of complex coupling coefficients, meaning complex entries of the adjacency matrix, which leads to asymmetric transport across the edges of

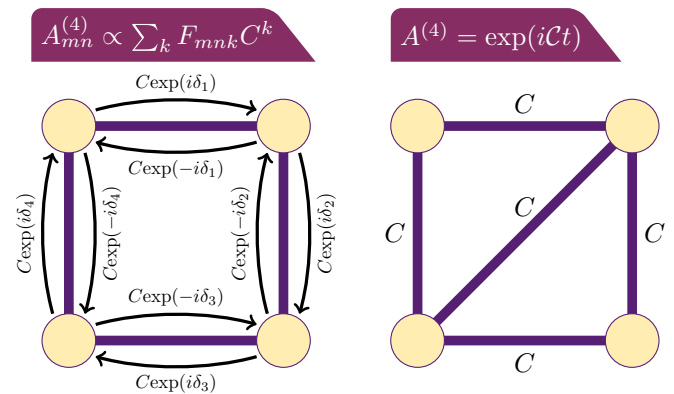


FIG. 2. Example of two similar linear couplers whose evolutions are easier to solve with different methods. For the closed tetramer with complex coupling (left), it is challenging to derive analytical expressions from $\exp(iCt)$, but the evolution of the bosonic operators can be readily represented as a series expansion in terms of the amplitude C (see Sec. II B). For the rhomboidal array (right), the exponential $\exp(iCt)$ can be calculated analytically for real coupling coefficients.

the graph [40,41] in the context of quantum random walks. Specifically, the dynamics in the N -mer is related to the problem of counting paths in a connected graph [42]. From Eq. (7), one sees that the expression enclosed in square brackets is formally equivalent to a sum over all the walks of length n leading to vertex m . Thus, Eq. (7) implies that the transformed mode a'_m results from adding the weights of all the paths leading to the m th vertex from the vertices associated with the modes a_j . This fact will be helpful to derive the explicit form of the transformations in Eq. (2) for the open and closed TB couplers in the next section.

B. Complex coupled tight-binding model

We now focus on the N -mode TB model with first-neighbor coupling. For the open case in Fig. 1(b), the Hamiltonian in Eq. (1) becomes

$$H = \hbar \sum_{j=1}^{N-1} (C_j a_j^\dagger a_{j+1} + C_j^* a_{j+1}^\dagger a_j), \quad (10)$$

where $C_j = C \exp(i\delta_j)$ is the complex coupling coefficient between the j th and the $(j+1)$ -th modes, being the amplitude C and the phases δ_j are real quantities. Equation (10) also describes the closed array shown in Fig. 1(c) by extending the sum to $j = N$ and taking $a_{N+1} = a_1$. Most physical descriptions using Eq. (10) consider real and identical coupling constants, i.e., $\delta_j = 0$, which implicitly assume time-reversal symmetry of the dynamics [40]. Here, we study a more general case exhibiting complex coupling coefficients with identical coupling amplitude between modes but different arbitrary phases δ_j . Note that the complex coupling terms in Eq. (10) are still Hermitian, so its dynamics differs from the non-Hermitian TB networks [33]. Instead, it exhibits asymmetrical coupling between connected nodes of the support graph, which gives rise to time-reversal symmetry breaking [43] and chiral quantum walks [40,41], whose actual effects strongly depend on the geometry and the parity of N [39].

The complex entries of the transformation matrix can be generally expressed as

$$A_{m,n}^{(N)} = \exp(-i\phi_{m,n}) \beta_{m,n}^{(N)}. \quad (11)$$

While this representation is valid for any complex value of the coefficients, it is not always possible to express it in an explicit form that is suitable for actual computations.

For the open array [Fig. 1(b)], an evaluation of the recursive terms in Eq. (5) leads to

$$\phi_{m,n} = \Delta_{m-1} - \Delta_{n-1}, \quad (12)$$

with $\Delta_k = \delta_1 + \delta_2 + \dots + \delta_k$ and $\Delta_0 = 0$. The (m, n) -th entry of the transformation matrix is found to have the general form

$$\begin{aligned} A_{m,n}^{(N)} &= \frac{2}{N+1} \exp[-i(\Delta_{m-1} - \Delta_{n-1})] \\ &\times \sum_{k=1}^N \exp\left[-2i \cos\left(\frac{k\pi}{N+1}\right) Ct\right] \\ &\times \sin\left(\frac{mk\pi}{N+1}\right) \sin\left(\frac{nk\pi}{N+1}\right). \end{aligned} \quad (13)$$

This expression can be derived from different approaches, discussed in Appendix C.

For the closed array [Fig. 1(c)], the translational symmetry of this case allows us to consider any mode as the first one. Then, we can deduce the structure of the transformation matrix $\bar{A}^{(N)}$, whose n th row has the same entries as the first but *cycled* by n positions:

$$\bar{A}^{(N)} = \begin{pmatrix} \bar{A}_{11}^{(N)} & \bar{A}_{12}^{(N)} & \cdots & \bar{A}_{1,N-1}^{(N)} & \bar{A}_{1N}^{(N)} \\ \bar{A}_{1N}^{(N)} & \bar{A}_{11}^{(N)} & \cdots & \bar{A}_{1,N-2}^{(N)} & \bar{A}_{1,N-1}^{(N)} \\ \vdots & \vdots & \ddots & \vdots & \vdots \\ \bar{A}_{1,2}^{(N)} & \bar{A}_{13}^{(N)} & \cdots & \bar{A}_{1N}^{(N)} & \bar{A}_{1,1}^{(N)} \end{pmatrix}. \quad (14)$$

Therefore, only the entries $\bar{A}_{1,n}^{(N)}$ are required to obtain the full matrix. Unlike the open N -mer, the matrix elements for the closed array are divided into several cases. For N even and n odd, with the condition $n = N/2 + 1$, we found

$$\bar{A}_{1,n}^{(N)} = 2 \sum_{l=0}^{\infty} \cos\left[\frac{N}{2}(2l+1)(\delta - \pi/2)\right] J_{N(2l+1)/2}(2Ct), \quad (15)$$

where the $J_{N(2l+1)/2}$ are the Bessel function of the first kind and $\delta = \delta_j$ (same phase for every coupling). The remaining cases are listed in Eq. (C27) of Appendix C. Circulant matrices, such as $\bar{A}^{(N)}$, are diagonalized by means of the discrete Fourier transform and, consequently, linear functions of them can be efficiently evaluated by a fast Fourier transform.

It is important to highlight the versatility of the previous formalism, since Eq. (11) holds for any set of coupling coefficients, beyond the two one-dimensional cases studied here. This allows us to extend our study to two-dimensional systems that can be mapped to a one-dimensional array (i.e., systems whose nodes can be properly enumerated and the coupling between them set accordingly), provided that the appropriate integer sequence or recurrence matrix is known. Remarkable examples are *flat-band lattices* whose dynamics can be addressed using a one-dimensional linear coupler [44,45].

III. APPLICATIONS

We use our previous results to describe the quantum evolution of many particles or excitations in N linearly coupled modes. We aim to quantify quantum correlations between particles through their evolution (both in the position and the quadrature space). While the time required to solve the single-particle problem scales linearly with the number of modes N , it grows exponentially with the maximum number of particles. Computing the evolution of such systems is generally hard. However, it can be significantly simplified using the expressions obtained in the previous section.

A. Method summary

Figure 3 summarizes the method we follow to efficiently compute the evolution of states or expectation values. We express the initial state as an operator $\hat{\Xi}$ acting over the vacuum state, where $\hat{\Xi}$ is written as a combination of terms containing

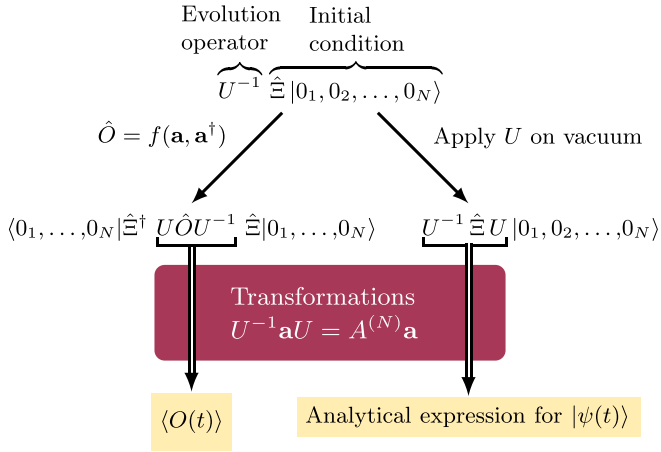


FIG. 3. Schematic of the method to compute the evolution of the expectation value of any observable expressible as an analytic function of \mathbf{a} and \mathbf{a}^\dagger (left) or the state of the system (right). Knowing the analytical form of the transformation matrix $A^{(N)}$, we can consider any initial state generated by an operator $\hat{\Xi}$ composed of sums and products of the operators a_j^\dagger .

powers of the creation and annihilation operators. For example, in Sec. III B, we study the evolution from a product of single-mode squeezed vacuum states $|\xi_1\rangle|\xi_2\rangle\cdots|\xi_N\rangle$, so the corresponding operator will be $\hat{\Xi} = \hat{S}_1(\xi_1)\hat{S}_2(\xi_2)\cdots\hat{S}_N(\xi_N)$, with $S_j(\xi_j)$ the squeezing operator on the mode j with squeezing parameter ξ_j . On the other hand, as a part of our study of two-particle correlations in Sec. III D, we require an initial state given by the superposition of Fock states $1/\sqrt{2}(|2_k\rangle + |2_\ell\rangle)$ so we use $\hat{\Xi} = 1/2[(a_k^\dagger)^2 + (a_\ell^\dagger)^2]$.

The evolution is calculated through $U = \exp(-iHt/\hbar)$. Depending on our goal, we choose between two different procedures. To obtain the state evolution, we operate with U on the vacuum state, using the fact that it remains unaffected by rotations, obtaining $U^{-1}\hat{\Xi}U$. Since the operator $\hat{\Xi}$ can be decomposed in sums and powers of the creation operators a_i , we can then use the identity

$$U^{-1}a_j^\dagger U = \sum_i A_{ji}^{(N)*} a_i^\dagger, \quad (16)$$

and then apply our main results, summarized in Appendix B and deduced in Appendix C. Specifically, we use Eq. (11) for the open arrays and Eq. (15) for the closed arrays. An arbitrary case can always be addressed by the exponential expression in Eq. (9) which, as discussed in Sec. II A, is not the optimal method in most cases. On the other hand, to compute the expectation value of an observable \hat{O} expressible as an analytic function of a and a^\dagger , the transformations Ua_jU^{-1} and $Ua_j^\dagger U^{-1}$ allow one to evaluate $U\hat{O}U^{-1}$. This method is versatile enough to address evolution from a wide variety of initial conditions, which could be a superposition of Fock states, squeezed-coherent states, and even photon-added (-subtracted) squeezed-coherent states [19,46–51].

B. Single-mode squeezing cancellation

The propagation of squeezed states through an open N -mer has been previously studied [35]. In particular, it has

been shown that for $N = 2$ and $N = 3$, an initial product of single-mode squeezed states can evolve into a state exhibiting multimode squeezing with suppressed single-mode squeezing [17,52]. This procedure allows one to induce multimode correlations among quantum fluctuations of different pairs of modes from a single-mode squeezed state. We use the mathematical tools developed here to generalize this phenomenon to an arbitrary $N > 3$. Let us consider that the initial state of the system is given by a product of single-mode squeezed vacuum states,

$$|\psi_0\rangle = \hat{S}_1(\xi_1)\hat{S}_2(\xi_2)\cdots\hat{S}_N(\xi_N)|0\rangle, \quad (17)$$

with $\hat{S}_j(\xi_j) = \exp[(\xi_j^* a_j^2 - \xi_j a_j^{\dagger 2})/2]$ the squeezing operator on the j th mode. As depicted in the diagram of Fig. 3, the state of the system after a time t is obtained by applying the unitary operator U^{-1} on the squeezing operators of the initial state and the inverse U on the vacuum, leading to

$$|\psi_t\rangle = \exp\left\{\frac{1}{2}\left[\sum_{j=1}^N a_j^2 \sum_{i=1}^N \xi_i^* (A_{ij}^{(N)})^2 + 2 \sum_{k=1}^{N-1} \sum_{j=k+1}^N a_k a_j \times \sum_{i=1}^N \xi_i^* A_{ik}^{(N)} A_{ij}^{(N)} - \text{H.c.}\right]\right\} |0_1, \dots, 0_N\rangle, \quad (18)$$

where the dependence on time t is implicit in the coefficients $A_{ij}^{(N)}$ of the transformation matrix obtained in Sec. II B. From the first term in this expression, it follows that a single-mode squeezing suppression fulfill the condition

$$\sum_{i=1}^N \xi_i^* (A_{ij}^{(N)})^2 = 0, \quad \forall j = 1, 2, \dots, N. \quad (19)$$

Let us consider real initial squeezing parameters. This assumption leads to a system of N equations and $N + 1$ unknowns: the N initial squeezing parameters and the propagation distance t at which the single-mode squeezing nullifies. However, since we are not interested in the exact amount of initial squeezing but in the relation between the squeezing parameters for all the modes, one squeezing parameter can be arbitrary, rendering the problem solvable. Furthermore, we can set the required initial distribution of squeezing to be symmetrical across the N -mer, i.e., squeezing in the j th and $(N + 1 - j)$ -th modes should be the same. In this way, Eq. (19) leads to a system of $(N + 1)/2$ equations ($N/2$ equations) for odd N (even N), with the same number of unknowns. Note that due to the linear independence of Eq. (19) and the columns of the transformation matrix, the sums $\sum_i \xi_i A_{ik}^{(N)} A_{ij}^{(N)}$ in the second term of Eq. (18) will not be null in general for any pair k, j when evaluated in the solutions ξ_i^* . Therefore, we can expect to find two-mode squeezing over different pairs of modes throughout the evolution where single-mode squeezing is suppressed.

We exemplify this with a pentamer ($N = 5$) having real first-neighbor coupling. By solving Eq. (19), we find that the squeezing values $\xi_1 = \xi_5 = 0.1$, $\xi_2 = \xi_4 = 0.25$, and $\xi_3 = 0.3$ suppress single-mode squeezing at $t = 0.640$, but not multimode squeezing. Figure 4 shows the squeezing dynamics for this case, along with analogous results for the enneamer ($N = 9$). At certain stages of the evolution, single-mode

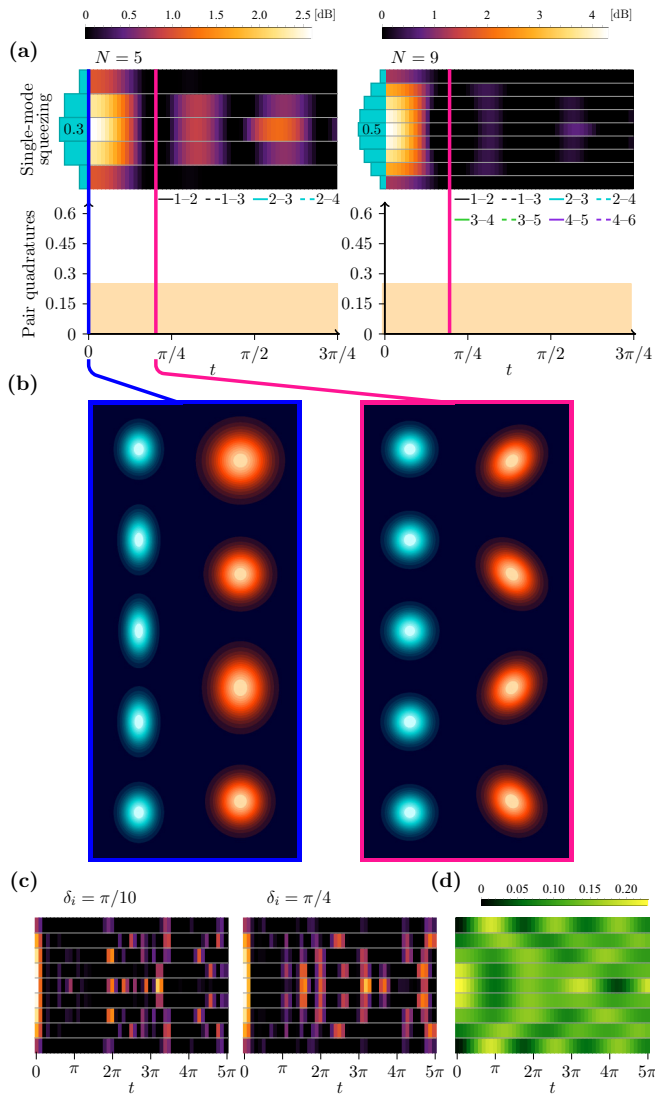


FIG. 4. Transition from single-mode to multimode squeezing in linear couplers. (a) Evolution of the single-mode squeezing degree for the pentamer (top left) and the enneamer (top right). Black regions indicate the absence of single-mode squeezing. The relation between the respective squeezing parameters ξ_i of the initial state is depicted by the horizontal blue bars, where we indicate the initial value at the center mode used in the simulations. The dynamics of the variance of two-mode quadratures for different pairs of modes is shown in the plots, where the orange region indicates squeezing. Vertical pink lines mark a distance where the state of the system exhibits multimode squeezing only. (b) Single-mode Wigner function (blue surfaces) and marginal distributions of the multimode Wigner function for the same pairs of quadratures (red surfaces) for $N = 5$. (c) Examples of the evolution of the squeezing degree in the enneamer when complex coefficients with identical phases $\delta_i \neq 0$ are considered. The values are in the same range shown by the bar in (a) for $N = 9$. (d) The particle number at each mode, here shown for the $N = 9$ case, is the same for any value of the coupling phases.

squeezing vanishes, while squeezing is observed in the variance of the two-mode quadratures between multiple pairs of modes. We confirm this by computing the single-mode and multimode Wigner functions at different values of t ,

shown for $N = 5$ in Fig. 4(b). The suppression of single-mode squeezing is clearly observed in the Wigner function of each mode (blue surfaces). Conversely, the marginal distributions of the multimode Wigner functions [17,53] become squeezed (red surfaces). When the maximal multimode squeezing is achieved, the single-mode states (in this case, per waveguide) become thermal [17].

Our results generalize previous ones, showing that N -mers can produce multimode squeezed states among arbitrary $N > 3$ modes from initially single-mode squeezed states. In addition, we computed the evolution of the squeezing degree (in dB) for complex coupling coefficients, i.e., $\delta_i \neq 0$. As shown by the examples in Fig. 4(c), single-mode squeezing cancellation, with the corresponding transition to multimode squeezing (not shown in the examples), still occurs for the studied phases, with the particular evolution of the squeezing degree being different for each case. Interestingly, the effect of the complex coupling is not reflected in the evolution of the particle number [presented in Fig. 4(d) for the enneamer], which is the same for all the values of δ_i under consideration.

C. Wigner function representation for propagating nonclassical states

Wigner functions are informationally complete graphic representations of the quantum states of single and multimode electromagnetic fields. Negative values in the Wigner function imply that the field is purely quantum without a classical counterpart [54,55]. Since its dynamics reflects the state evolution, the Wigner representation is useful for readily identifying emerging or vanishing quantum features [56,57], an otherwise challenging mathematical task. The results presented in Sec. II are particularly useful to track the variation of the multimode Wigner function describing nonclassical states of the system.

As an example, we study the propagation of initial states obtained by adding (subtracting) a single excitation to (from) a nondisplaced Gaussian state and examine the Wigner function dynamics. In recent articles, a rather simple expression for the Wigner function $W_G(Y)$ of a single-photon added and subtracted Gaussian state was presented [22,34], which uses the symplectic representation of the phase space. In this framework, we associate the in-phase and out-of-phase components of the ℓ th mode amplitude with two elements, $e^{(\ell)}$ and $Je^{(\ell)}$, in a *symplectic basis*:

$$\mathcal{E}^s = \{e^{(1)}, \dots, e^{(N)}, Je^{(1)}, \dots, Je^{(N)}\}, \quad (20)$$

where J is a $2N \times 2N$ matrix fulfilling $J^2 = -\mathbb{I}$ and $(f_1)(Jf_2) = (-f_2)(Jf_1)$ for any f_1 and f_2 linear combinations of the symplectic basis in \mathbb{R}^{2N} , sometimes called the *symplectic form*. The operators that annihilate and create an excitation in the mode f are denoted by $a(f)$ and $a^\dagger(f)$ and can be defined in terms of quadrature operators as

$$a(f) = [Q(f) - iQ(Jf)]/2, \quad a^\dagger(f) = [Q(f) + iQ(Jf)]/2. \quad (21)$$

In order to use our expressions for the transformation matrix $A^{(N)}$ with the symplectic formalism, we set the correspondence $a_j = a(e_j)$. Since the quadrature operators are linear, i.e., $Q(\alpha f_1 + \beta f_2) = \alpha Q(f_1) + \beta Q(f_2)$ and

$a(Jf) = -ia(f)$, we can describe the evolution $a'_j = Ua_jU^{-1}$ as a transformation of the corresponding mode in the symplectic space,

$$a'_j = \sum_{\ell=1}^N A_{j,\ell}^{(N)} a_\ell = a \left\{ \sum_{\ell=1}^N [\text{Re}(A_{j\ell}^{(N)})e_\ell + \text{Im}(A_{j\ell}^{(N)})Je_\ell] \right\},$$

$$a_j^{\dagger'} = a^\dagger \left\{ \sum_{\ell=1}^N [\text{Re}(A_{j\ell}^{(N)})e_\ell - \text{Im}(A_{j\ell}^{(N)})Je_\ell] \right\}. \quad (22)$$

Upon this equivalence, it is possible to keep track of how the characteristic function and the Wigner function of the system are transformed. Its definition, as derived in Ref. [22], involves two key elements. The first one is the covariance matrix V , whose (i, j) -th entry is the symmetrized covariance between quadrature operators $Q(\mathcal{E}_i^s)$ and $Q(\mathcal{E}_j^s)$ evaluated in the basis e^s . Following the same principle as in Eq. (22), the entry V'_{ij} after evolution is given by

$$V'_{ij} = \frac{1}{2}(\Delta Q'(\mathcal{E}_i^s)\Delta Q'(\mathcal{E}_j^s) + \Delta Q'(\mathcal{E}_j^s)\Delta Q'(\mathcal{E}_i^s)), \quad (23)$$

with

$$Q'(\mathcal{E}_i^s) = a[(\text{Re } \mathbf{A}^T \oplus \text{Im } \mathbf{A}^T)\mathcal{E}_i^s] + a^\dagger[(\text{Re } \mathbf{A}^T \oplus -\text{Im } \mathbf{A}^T)\mathcal{E}_i^s].$$

This matrix captures the influence of the Gaussian component of the initial state on the evolution of the system. Second, consider that a single excitation is added, the added or subtracted excitation in a mode is described by a vector g in the symplectic basis. The additional correlations induced by this excitation are captured by the following matrix acting on the space \mathbb{R}^{2N} :

$$\mathcal{A}^\pm = 2 \frac{(V \pm 1)(P_g + P_{Jg})(V \pm 1)}{\text{tr}[(V \pm 1)(P_g + P_{Jg})]}, \quad (24)$$

where P_g and P_{Jg} are the projectors on vectors g and Jg , respectively. Its evolution under U is obtained by using Eq. (23) and transforming g accordingly. Using these definitions (cf. Ref. [22]), we can express the Wigner function of the evolved state as

$$W^\pm(Y) = Z^\pm(Y)W_G(Y), \quad (25)$$

with

$$Z^\pm(Y) = \frac{1}{2}[Y^T V^{-1} \mathcal{A}^\pm V'^{-1} Y - \text{tr}(V'^{-1} \mathcal{A}^\pm) + 2], \quad (26)$$

where Y is a vector expressed in the base \mathcal{E}^s which spans the quadrature space, and $W_G(Y)$ is the Wigner function of the nondisplaced Gaussian state given by

$$W_G(Y) = \frac{1}{(2\pi)^N \sqrt{\det V'}} \exp\left(-\frac{1}{2}Y^T V'^{-1} Y\right). \quad (27)$$

In Fig. 5, we present two illustrative examples showing the effect of adding a single excitation to the product of single-mode squeezed states studied in Sec. III B for the open pentamer ($N = 5$). We observe that when the excitation is added to a single mode, it results in the expected negativity of the corresponding Wigner function around the center of the phase space. As the system evolves, dips appear in the

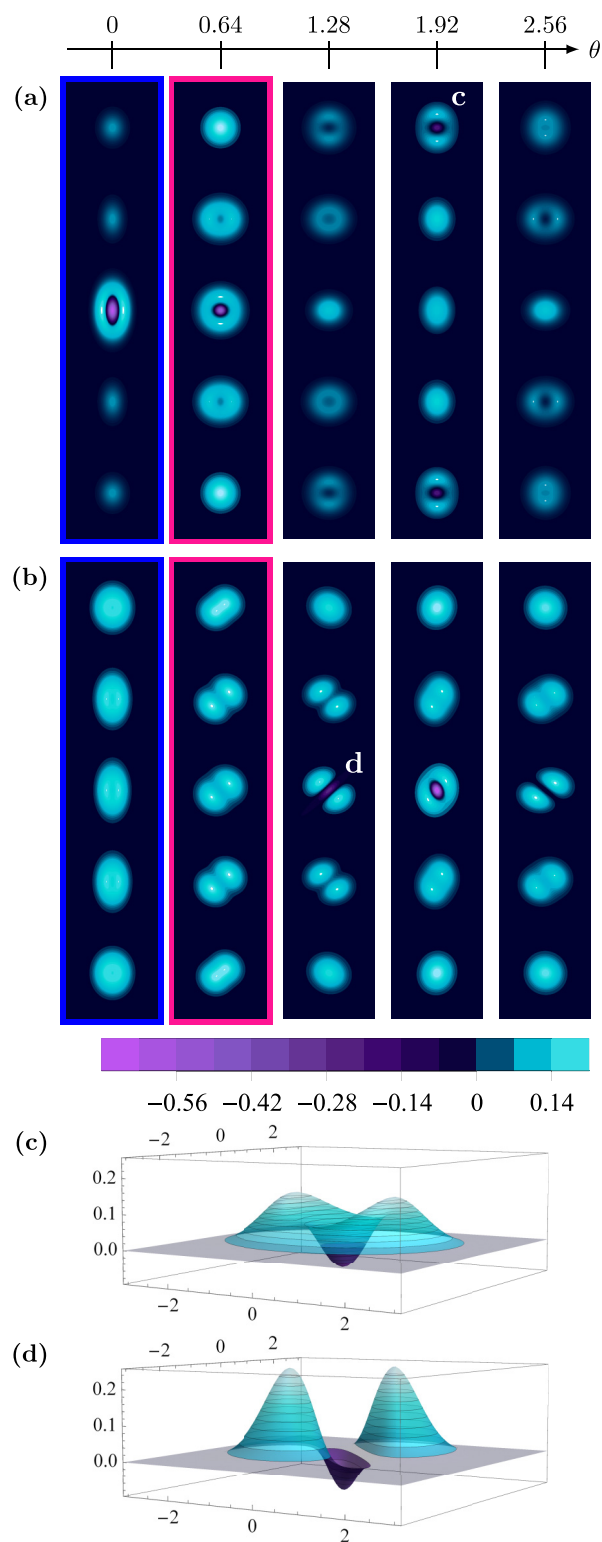


FIG. 5. Evolution of the Wigner function for each mode in the pentamer when a single excitation is added to the initial state, which is the same product of single-mode squeezed states as in Sec. III B. The excitation is added in (a) the mode a_3 and (b) in a uniform superposition of the five modes. Blue and pink frames indicate the same stages as in Fig. 4. Three-dimensional plots in (c) and (d) show two illustrative examples of different evolved states, also indicated in the upper graphs.

Wigner functions of the adjacent modes, so even the functions of the edge modes exhibit a negative region at some point. On the other hand, when the single excitation is added as a uniform superposition in all the modes [Fig. 5(b)], it does not lead to negative regions for any mode at the initial stage; interestingly, the Wigner function's distributions rotate through the evolution, with noticeable negativity regions appearing for the central mode.

These examples show how highly non-Gaussian states arise during evolution, starting from products of quasi-Gaussian states. The symplectic space representation of field evolution allows studying different state superpositions added to a wide class of Gaussian states beyond our demonstrative results. Knowing the exact form of the Wigner function is crucial for applications such as computing the Cramer-Rao bound [25,58] for measuring phase shifts in a particular mode, thus providing a reliable estimation of the metrological improvement when using non-Gaussian input states.

D. Effect of phase disorder on quantum correlations

As a final application of our analytic results presented in Sec. II, we now study two-particle cross correlations after propagation through an N -mer, highlighting the quantum properties of the propagating fields. In particular, the study of photon pairs propagating through waveguide arrays shows that the interference in the N -mode system gives rise to photon bunching resembling the Hong-Ou-Mandel effect [13]. In the following, we study how this behavior is affected by decoherence arising from the random variation of the complex phases in the coupling coefficients. N -mode couplers exhibiting random amplitudes or *weights* of the coupling constants are known to produce Anderson localization, extensively studied. However, the effect of disorder in the phases of the coupling coefficients remains relatively unexplored.

Depending on the observable, two-particle states suffice to manifest the quantum nature of the system. A suitable measurement to reveal it is the two-particle correlation function Γ_{mn} , related to the probability of detecting a particle at each mode m and n ,

$$\Gamma_{mn} = \langle a_m^\dagger a_n^\dagger a_m a_n \rangle. \quad (28)$$

We are interested in computing the dynamics of the correlation $\Gamma_{mn}(t)$ for a state $|\psi_t\rangle$.

First, let us consider an initial two-photon state of the form $|1_{k_0}\rangle|1_{k_0+1}\rangle$ for two adjacent central modes k_0 and $k_0 + 1$, leading to

$$|\psi_t\rangle = U^{-1}|1_{k_0}\rangle|1_{k_0+1}\rangle = a_{k_0}^\dagger a_{k_0+1}^\dagger |0\rangle. \quad (29)$$

Substituting in Eq. (28) and using the result of Eq. (13), we obtain

$$\begin{aligned} \Gamma_{mn}(t) &= |A_{k_0,m}^{(N)} A_{k_0+1,n}^{(N)} + A_{k_0,n}^{(N)} A_{k_0+1,m}^{(N)}|^2 \\ &= \frac{1}{2} |\beta_{k_0,m}^{(N)} \beta_{k_0+1,n}^{(N)}|^2 + \frac{1}{2} |\beta_{k_0,n}^{(N)} \beta_{k_0+1,m}^{(N)}|^2 \\ &\quad + \beta_{k_0,m}^{(N)} \beta_{k_0+1,n}^{(N)*} \beta_{k_0,n}^{(N)*} \beta_{k_0+1,m}^{(N)} \exp[-i(\phi_{k_0,m} \\ &\quad + \phi_{k_0+1,n} - \phi_{k_0,n} - \phi_{k_0+1,m})] + \text{H.c.}, \quad (30) \end{aligned}$$

where we have used the notation introduced in Sec. II B in order to make explicit the dependence of Γ_{mn} on phases δ_j , which is then contained in the exponential term in Eq. (30). By noticing that $\phi_{j,m} - \phi_{j,n} = \phi_{n,m}$ and $\phi_{m,n} = -\phi_{n,m}$, we see that the argument in the exponential cancels, so Γ_{mn} is independent of phases δ_j . Accordingly, decoherence does not affect the dynamics of a product state since it does not exhibit coherence in the form of interference between two modes. Therefore, for any complex coupling phases, the evolution of $|1_{k_0}\rangle|1_{k_0+1}\rangle$ leads to the well-known bunching effect obtained from two-particle product states [13,14], where both particles are most likely to end in the same mode, as shown in Fig. 6(a). Note that the dynamics of the product state in the N -mer saturates the Cauchy-Schwartz inequality $\Gamma_{mn} < \sqrt{\Gamma_{mm}\Gamma_{nn}}$ but never violates it, as shown in Fig. 6(b).

Let us now consider that the system is initially in a superposition of two-photon states in modes k and ℓ , i.e.,

$$|\psi_0\rangle = \frac{1}{\sqrt{2}}(|2_k\rangle + |2_\ell\rangle). \quad (31)$$

The state after time t is given by

$$|\psi_t\rangle = \frac{1}{\sqrt{2}}[(a'_k)'^2 + (a'_\ell)'^2]|0\rangle. \quad (32)$$

Replacing Eqs. (13) and (32) in Eq. (28), we obtain

$$\begin{aligned} \Gamma_{mn}(t) &= |A_{k,m}^{(N)} A_{k,n}^{(N)} + A_{\ell,m}^{(N)} A_{\ell,n}^{(N)}|^2 = |\beta_{k,m}^{(N)} \beta_{\ell,n}^{(N)}|^2 + |\beta_{k,n}^{(N)} \beta_{\ell,m}^{(N)}|^2 \\ &\quad + \beta_{k,m}^{(N)} \beta_{\ell,n}^{(N)*} \beta_{k,n}^{(N)*} \beta_{\ell,m}^{(N)} 2 \cos(2\phi_{k,\ell}) + \text{H.c.} \quad (33) \end{aligned}$$

Unlike the product state, the initial superposition in Eq. (31) leads to a final state depending on the phases δ_j of the coupling coefficients. If $|\psi_0\rangle$ is composed of only two adjacent modes k_0 and $k_0 + 1$, the cosine in Eq. (33) simplifies to $\cos(2\delta_{k_0})$. In this case, a disorder in the coefficient phases reduces to δ_{k_0} varying randomly with a normal distribution of variance ϵ centered around $\delta_{k_0} = 0$. The width ϵ defines the degree of disorder. The average can be computed by direct integration, leading to

$$\begin{aligned} \Gamma_{mn}(t) &= |\beta_{k_0,m}^{(N)} \beta_{k_0+1,n}^{(N)}|^2 + |\beta_{k_0,n}^{(N)} \beta_{k_0+1,m}^{(N)}|^2 \\ &\quad - \exp(-2\epsilon^2) \beta_{k_0,m}^{(N)} \beta_{k_0+1,n}^{(N)*} \beta_{k_0,n}^{(N)*} \beta_{k_0+1,m}^{(N)} + \text{H.c.} \quad (34) \end{aligned}$$

In Figs. 6(c) and 6(d), we present the two-photon correlation function at time $t_f = 3\pi/4$ for different decoherence degrees (normal distribution of width ϵ). For $\epsilon = 0$ (no decoherence, identical and real coupling coefficients), a superposition of two-photon states in two adjacent modes $k = k_0$ and $\ell = k_0 + 1$ leads to the expected behavior for the correlations shown in Fig. 6(c), with each of the photons ending in distant modes, instead of the bunching obtained if both particles start in a product state. This effect is due to the interference expressed by the last term in Eq. (34). As we raise ϵ to introduce disorder in the phases δ_j , we observe how this behavior is gradually suppressed, and the output correlation becomes similar to the one obtained from a macroscopic or classical state. Again, this can be understood from Eq. (34) since the term accounting for quantum interference decays as $\exp(-2\epsilon^2)$. In fact, for $\epsilon = \pi$ [Fig. 6(e)],

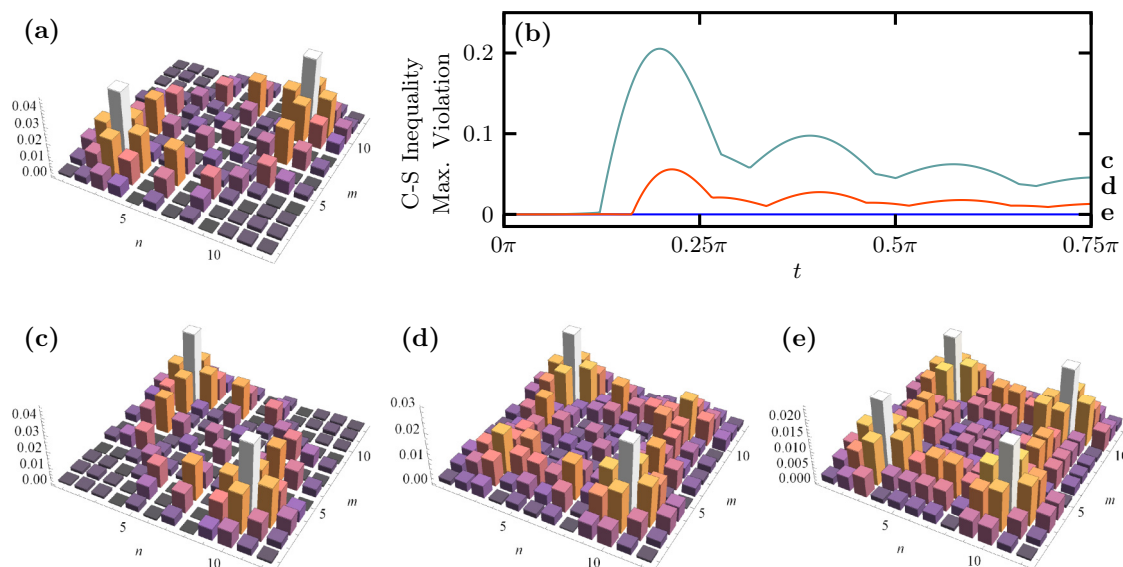


FIG. 6. Two-particle correlations after evolution up to $t_f = 3\pi/4$ from different initial states. (a) Initial state given by a product of single-particle states in adjacent middle modes, with real coupling. (b) Maximum violation of the Cauchy-Schwartz inequality. Corresponding cases are indicated by the letter next to the curves. (c) Evolution from a two-particle state in superposition over the adjacent center modes, $(|2_k\rangle + |2_\ell\rangle)/\sqrt{2}$, for equal and real coefficients $\epsilon = 0$. The same is shown in (d) for $\epsilon = 0.55\pi$ and (e) for $\epsilon = \pi$. Results are averaged over 100 realizations.

the correlation matrix exhibits a four-peak pattern similar to the one obtained from an initial state $|2\rangle_{k_0}$, which is a simple product of two single-photon distributions without coherence [13]. Interestingly, this is also reflected by a violation of the Cauchy-Schwartz inequality. Figure 6(b) shows the maximum violation as a function of t for the scenarios under consideration. Since this inequality sets an upper bound for classical correlations [59], its violation indicates quantum correlations. We observe that when the system evolves from an initial superposition, the inequality is violated as far as the decoherence degree ϵ is low; as this increases and the interference is suppressed, the maximum violation gradually decays until the system just saturates the Cauchy-Schwartz inequality for large ϵ . Such behavior evidences the fragility of quantum properties under decoherence, in this case, induced by random phases in the coupling coefficient.

The analytic solution of the TB model with complex coefficients allowed us to describe a previously almost unexplored decoherence mechanism, where quantum correlations wash out after propagation through an N -mer with random coupling phases. More generally, the description allows for simple expressions describing higher-order spatial correlation between modes, an otherwise challenging computational task.

IV. BENCHMARK

The standard procedure for solving the evolution of quantum systems often involves employing a basis function set spanning the Hilbert space, diagonalizing the Hamiltonian matrix, and using tensor products and partial traces to derive the desired expectation values. This procedure is challenging unless the dimension of the Hilbert space is small [60]. The computational complexity grows exponentially with the

number of modes [13], emphasizing the need for efficient computational tools.

We now compare solving the N -mer evolution with our analytical expressions versus numerical solvers of the Schrödinger equation. Figure 7 compares the computation time required to calculate the evolution from initial products of squeezed vacuum states with real squeezing parameters (similar to the initial states used in Sec. III B) using the respective toolboxes for MATLAB, JULIA, PYTHON, and our analytical results. Solutions in these languages were computed with a maximum particle number equal to 40, which leads to a respective Hilbert space of size 1600 for $N = 2$, 64 000 for $N = 3$, 2 560 000 for $N = 4$, and 102 400 000 for $N = 5$.

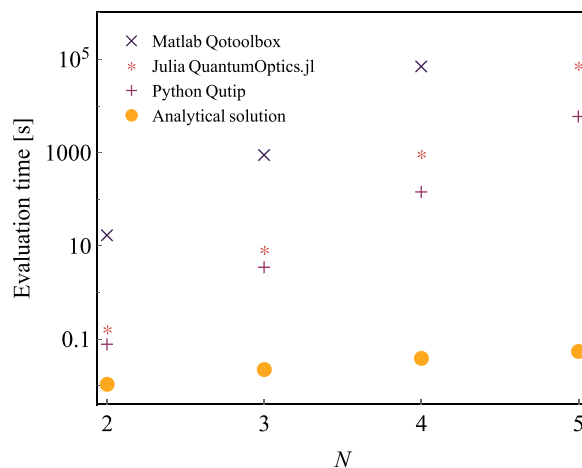


FIG. 7. Comparison of the average time required to compute the evolution of squeezed initial states in the N -mer using numerical integration in different languages and the analytical results of Sec. II A.

All calculations were carried out on a laptop computer with an 8-core Intel i7 processor operating at a clock speed of 2.80 GHz, and 16 GB of DDR4 RAM. The numerical values of the analytical expression were obtained by implementing the respective functions in C++. The solutions for different numerical tools agree with each other, differing only on the computational time. The results showcase a substantial advantage in average computation time when utilizing analytical expressions, reaching up to six orders of magnitude difference for the pentamer case. We omit tests for larger systems due to RAM limitations, which introduce significant inconsistencies in computation time for numerical approaches, where resource allocation becomes crucial. In fact, for $N > 6$, the equations could not be solved numerically, even on a computer with 128 GB RAM.

V. SUMMARY AND OUTLOOK

Initially proposed to calculate band structures in solids, the tight-binding model describes several analogous systems, such as optical lattices with cold atoms, light propagating in phononic crystals, surface waves, topological insulators, and quantum random walks. Despite its conceptual simplicity and broad applicability, many cases lack analytical solutions. We find exact analytical solutions for the spatial evolution of arbitrary quantum states in one-dimensional tight-binding models with complex coupling constants of equal amplitudes and arbitrary phases. Our results have profound implications for understanding transport dynamics and quantum correlations in real space, enabling us to describe these phenomena within an analytical framework.

Our analytic solutions provide a considerable computational advantage over standard numerical solvers regarding efficiency and accuracy. In particular, we compared performances when solving the Schrödinger equation to compute spatial propagation and correlations in large systems involving many particles for nontrivial initial conditions, such as products of single-mode squeezed states. Such a computation advantage could facilitate studying the effect of losses in the propagation of light and quantum correlations through quantum Monte Carlo methods, which require simulating many trajectories.

To demonstrate the generality and practicality of our analytic results, we have applied them to the study of quantum light propagation in multimode linear couplers. We have showcased the generalization of multimode squeezing formation from single-mode squeezed states and efficiently computed the dynamics of the Wigner function of single excitation added (subtracted) to (from) a displaced many-mode Gaussian state, revealing the emergence and propagation of highly non-Gaussian states. Finally, we also studied the evolution of two-particle cross correlations, highlighting the propagation of quantum properties of the fields. In particular, we analytically showed that decoherence arising from phase disorder, that is, random variation of the complex phases in the coupling coefficients, leads to a quantum-to-classical transition in the two-particle correlation function.

Although our main emphasis is on a mathematical method to obtain analytical solutions of the tight-binding model, we

also provide physical insight in its application to interesting examples. However, we hope that our results may prove valuable in the study of other physical systems described by the tight-binding model, such as other geometric configurations. In this regard, analytic results such as ours could have an impact that extends as broadly as the tight-binding model itself.

ACKNOWLEDGMENTS

This work was supported in part by ANID-PAI Grants No. 77180003 and No. 77190033, FONDECYT Grants No. 1230897, No. 11200192, No. 1231940 and No. 1230586. ANID Doctoral Fellowship Grant No. 21192248, and ANID - Millennium Science Initiative Program Grant No. ICN17_012. A.D. and P.S. acknowledges support as a CIFAR Azrieli Global Scholar in the Quantum Information Science Program.

APPENDIX A: COUPLING MATRIX

The transformed mode a'_m according to Eq. (4) is given by

$$a'_m = \sum_{n=0}^{\infty} \frac{1}{n!} \left(\frac{it}{\hbar} \right)^n [H, a_m]_n, \quad (\text{A1})$$

where

$$[H, a_m]_n = \sum_{j=1}^N \Lambda_j^{(n)} a_j. \quad (\text{A2})$$

Now we calculate the $(n+1)$ -th commutator between H and a_m , obtaining

$$[H, a_m]_{n+1} = \left[H, \sum_{l=1}^N \Lambda_l^{(n)} a_l \right]. \quad (\text{A3})$$

Using the general Hamiltonian given by Eq. (1), in the equation above, the commutator becomes

$$[H, a_m]_{n+1} = - \sum_{l=1}^N \hbar \Lambda_l^{(n)} \left[\sum_{(j,k)} (C_{j,k} \delta_{lj} a_k + C_{j,k}^* \delta_{lk} a_j) \right]. \quad (\text{A4})$$

Since the sum is constrained to modes j and k connected to mode l , we obtain

$$[H, a_m]_{n+1} = - \sum_{l=1}^N \hbar \Lambda_l^{(n)} \left[\sum_{(j(l),k(l))} (C_{l,k(l)} a_{k(l)} + C_{j(l),l}^* a_{j(l)}) \right]. \quad (\text{A5})$$

Using the fact that $C_{i,j}^* = C_{j,i}$ and by exchanging the summation over Eq. (A5), we find, for the $(n+1)$ -th commutator,

$$[H, a_m]_{n+1} = \sum_{j=1}^N \left(-\hbar \sum_{l(j)} \Lambda_{l(j)}^{(n)} C_{l(j),j} \right) a_j. \quad (\text{A6})$$

From (A6), we can see that the $\Lambda_j^{(n+1)}$ coefficients are recursively related to the $\Lambda_{l(j)}^{(n)}$ coefficients by the iterative rule,

$$\Lambda_j^{(n+1)} = -\hbar \sum_{l(j)} C_{l(j),j} \Lambda_{l(j)}^{(n)}. \quad (\text{A7})$$

This can be cast as a matrix equation,

$$\vec{\Lambda}_{n+1} = -\hbar \mathcal{C}^\top \vec{\Lambda}_n, \quad (\text{A8})$$

where

$$\mathcal{C} = \begin{pmatrix} 0 & C_{1,2} & \cdots & C_{1,N} \\ C_{1,2}^* & 0 & \cdots & C_{2,N} \\ \vdots & \vdots & \ddots & \vdots \\ C_{1,N}^* & C_{2,N}^* & \cdots & 0 \end{pmatrix}, \quad \vec{\Lambda}_n = \begin{pmatrix} \Lambda_1^{(n)} \\ \Lambda_2^{(n)} \\ \vdots \\ \Lambda_N^{(n)} \end{pmatrix}. \quad (\text{A9})$$

The recursive relation between the Λ coefficients in Eq. (A9) guides us to apply \mathcal{C}^\top n times over an initial condition $\vec{\Lambda}_0$ (which depends on the transformed mode a_m). By doing this operation, the recursive commutator $[H, a_m]_n$ results in

$$[H, a_m]_n = \sum_{j=1}^N \hat{e}_j^\top (-\hbar \mathcal{C}^\top)^n \hat{e}_m a_j. \quad (\text{A10})$$

By inserting (A10) in (A1), we obtain, for the transformed modes,

$$a'_m = \sum_{n=1}^{\infty} \frac{1}{n!} \left(\frac{it}{\hbar} \right)^n \left[\sum_{j=1}^N \hat{e}_j^\top (-\hbar \mathcal{C}^\top)^n \hat{e}_m a_j \right],$$

$$a'_m = \sum_{j=1}^N \hat{e}_j^\top \exp(-it\mathcal{C}^\top) \hat{e}_m a_j. \quad (\text{A11})$$

Thereby, transformed modes a' are related to the modes a_j through the matrix relation

$$\begin{pmatrix} a'_1 \\ a'_2 \\ \vdots \\ a'_N \end{pmatrix} = \exp(-it\mathcal{C}) \begin{pmatrix} a_1 \\ a_2 \\ \vdots \\ a_N \end{pmatrix}. \quad (\text{A12})$$

APPENDIX B: MAIN RESULTS

In this section, we summarize the main results obtained when evaluating the matrix

$$A = \exp(-it\mathcal{C}), \quad (\text{B1})$$

where \mathcal{C} is the coupling coefficient matrix for closed and open arrays. A detailed derivation of the coefficients of A can be found in Appendix C.

1. Closed array

In this case, the matrix A turns out to be circulant. Thereby, the n th row has the same entries as the first row, but cycled by n positions. The first-row coefficients of matrix A for a N -mer with first-neighbor coupling constants given by $C_j = C \exp(i\delta)$, with C and δ arbitrary but constant, are given by

the expression

$$\vec{A}_{1,n}^{(N)} = \begin{cases} \alpha_N^{(1)}, & N \text{ odd}, \quad n = 1 \\ \alpha_{N,n}^{(2)}, & N \text{ odd}, \quad n \leq (N+1)/2 \\ \mathcal{P}_c \alpha_{N,N-n+2}^{(2)}, & N \text{ odd}, \quad n > (N+1)/2 \\ \alpha_N^{(0)}, & N \text{ even}, \quad n = 1 \\ \alpha_{N,n}^{(2)}, & N \text{ even}, \quad n \leq N/2 \\ \alpha_{N,n}^{(3)}, & N \text{ even}, \quad n = \frac{N}{2} + 1, \quad n \text{ odd} \\ \alpha_{N,n}^{(4)}, & N \text{ even}, \quad n = \frac{N}{2} + 1, \quad n \text{ even} \\ \alpha_{N,N-n+2}^{(2)*}, & N \text{ even}, \quad n > \frac{N}{2} + 1, \quad n \text{ odd} \\ -\alpha_{N,N-n+2}^{(2)*}, & N \text{ even}, \quad n > \frac{N}{2} + 1, \quad n \text{ even}, \end{cases} \quad (\text{B2})$$

where the $\alpha_{N,n}$ functions are given by

$$\alpha_N^{(0)} = -J_0(2Ct) + 2 \sum_{l=0}^{\infty} \cos[lN(\delta - \pi/2)] J_{lN}(2Ct),$$

$$\alpha_N^{(1)} = -J_0(2Ct) + 2 \sum_{l=0}^{\infty} \{ \cos[2lN(\delta - \pi/2)] J_{2lN}(2Ct) + i \sin[(2l+1)N(\delta - \pi/2)] J_{(2l+1)N}(2Ct) \},$$

$$\alpha_{N,n}^{(2)} = \sum_{l=1}^{\infty} \sigma_{N,n,l} \exp[(-1)^{l+1} b_l(N, n)(\delta - \pi/2)i] \times J_{b_l}(2Ct),$$

$$\alpha_{N,n}^{(3)} = 2 \sum_{l=0}^{\infty} \cos\left[\frac{N}{2}(2l+1)(\delta - \pi/2)\right] J_{N(2l+1)/2}(2Ct),$$

$$\alpha_{N,n}^{(4)} = 2i \sum_{l=0}^{\infty} \sin\left[\frac{N}{2}(2l+1)(\delta - \pi/2)\right] J_{N(2l+1)/2}(2Ct), \quad (\text{B3})$$

with a parity conjugation operator

$$\mathcal{P}_c e^{in\delta} = \begin{cases} -e^{-in\delta}, & n \text{ odd} \\ e^{-in\delta}, & n \text{ even}. \end{cases} \quad (\text{B4})$$

The Bessel functions $J_k(2Ct)$ are of the first kind and the special sign function $\sigma_{N,n,l}$ is given by

$$\sigma_{N,n,l} = \begin{cases} \sigma_1[b_l(N, n)], & N \text{ odd}, \quad n \text{ even} \\ \sigma_2[b_l(N, n)], & N \text{ odd}, \quad n \text{ odd} \\ (-1)^{l+1}, & N \text{ even}, \quad n \text{ even} \\ 1, & N \text{ even}, \quad n \text{ odd}, \end{cases}$$

$$\sigma_1(b_l(N, n)) = \begin{cases} -1, & b_l(N, n) = 2N - n + 1 \pmod{2N} \\ 1 & \text{otherwise,} \end{cases}$$

$$\sigma_2[b_l(N, n)] = \begin{cases} -1, & b_l(N, n) = N - n + 1 \pmod{N} \\ 1 & \text{otherwise,} \end{cases}, \quad (\text{B5})$$

where indexes $b_l(N, n)$ are defined by the set

$$b_l(N, n) = \{k \in \mathbb{N} \mid k = n - 1 \vee N - n + 1 \pmod{N}\}. \quad (\text{B6})$$

2. Open array

In this case, the coefficients of matrix A for a N -mer with first-neighbor coupling constants given by $C_j = C \exp(i\delta_j)$, with C and δ_j arbitrary, are given by the expression

$$A_{m,n}^{(N)} = \frac{2}{N+1} \sum_{k=1}^N \exp\left[-2i \cos\left(\frac{k\pi}{N+1}\right) Ct\right] S_{mnk}, \quad (\text{B7})$$

where

$$S_{mnk} = \exp\left\{-i\left[\frac{\pi}{2}(m-n) + \Delta_{m-1} - \Delta_{n-1}\right]\right\} \times \sin\left(\frac{mk\pi}{N+1}\right) \sin\left(\frac{nk\pi}{N+1}\right) \quad (\text{B8})$$

and

$$\Delta_n = \delta_1 + \delta_2 + \dots + \delta_n. \quad (\text{B9})$$

APPENDIX C: DERIVATION

1. Mathematical context: Overview

We consider a lattice formed by an N nearest-neighbor evanescently coupled bosonic single mode described by the quantum Hamiltonian

$$H = \hbar \sum_{j=1}^{N-1} (C_j a_j^\dagger a_{j+1} + C_j^* a_{j+1}^\dagger a_j), \quad (\text{C1})$$

where a_j (a_j^\dagger) is the annihilation (creation) operator of an excitation in the j th mode and $C_j = C \exp(i\delta_j)$ is the complex coupling coefficient between the j th and the $(j+1)$ -th modes, with C and δ_j real numbers. It is worth noting that the standard model used for waveguide arrays or Bose-Einstein condensates in periodical lattices, which considers real coupling constants, is obtained by taking $\delta_j \equiv 0$, i.e., $C_j \equiv C$.

Closed analytic solutions for the elements of the transformation matrix $A^{(N)}$, given by Eq. (9), were obtained for $N = 2$ [52] and $N = 3$ [17]. For $N = 4$, the transformation element that accompanies a_2 in the evolution of a_1 (that is, a_1'), namely, $A_{1,2}^{(4)}$, can be obtained in terms of the series expansion of Eq. (A1), resulting in

$$A_{1,2}^{(4)} = -ie^{i\delta_1} \left[(Ct) - \frac{2}{3!}(Ct)^3 + \frac{5}{5!}(Ct)^5 - \frac{13}{7!}(Ct)^7 + \frac{34}{9!}(Ct)^9 - \frac{89}{11!}(Ct)^{11} + \frac{233}{13!}(Ct)^{13} - \dots \right]. \quad (\text{C2})$$

The coefficients in Eq. (C2) exhibit an interesting property; they are the odd terms of the Fibonacci succession, so the series can be rewritten as

$$A_{1,2}^{(4)} = -ie^{i\delta_1} \sum_{j=0}^{\infty} \frac{(-1)^j}{(2j+1)!} S_{2j+1}(Ct)^{2j+1}. \quad (\text{C3})$$

TABLE I. Sequences in the coefficients $\beta_{1,1}$ and $\beta_{N,N}$ for different N . We show the respective OEIS code and generating function.

N	Sequence	OEIS	$G_N(x)$
2	1,1,1,1,1,1,...	A000012	$\frac{1}{1-x}$
3	1,1,2,4,8,16,32,...	A011782	$\frac{1-x}{1-2x}$
4	1,1,2,5,13,34,89,233,...	A001519	$\frac{1-2x}{1-3x+x^2}$
5	1,1,2,5,14,41,122,365,...	A124302	$\frac{1-3x+x^2}{1-4x+3x^2}$
6	1,1,2,5,14,42,131,417,...	A080937	$\frac{1-4x+3x^2}{1-5x+6x^2-x^3}$
7	1,1,2,5,14,42,132,428,...	A024175	$\frac{1-5x+6x^2-x^3}{1-6x+10x^2-4x^3}$
8	1,1,2,5,14,42,132,429,...	A080938	$\frac{1-6x+10x^2-4x^3}{1-7x+15x^2-10x^3+x^4}$

By means of Binet's Fibonacci Number formula [61], the j th term of the succession is expressed as

$$S_j = \frac{1}{\sqrt{5}} \left[\left(\frac{1+\sqrt{5}}{2} \right)^j - \left(\frac{1-\sqrt{5}}{2} \right)^j \right]. \quad (\text{C4})$$

Using Eq. (C4) in Eq. (C3), we finally obtain an analytic expression for $A_{1,2}^{(4)}$,

$$A_{1,2}^{(4)} = -\frac{ie^{i\delta_1}}{\sqrt{5}} \left[\sin\left(\frac{1+\sqrt{5}}{2} Ct\right) + \sin\left(\frac{\sqrt{5}-1}{2} Ct\right) \right]. \quad (\text{C5})$$

The previous calculation of $A_{1,2}^{(4)}$ is essential to acquire a comprehensive understanding of the procedure to achieve general analytic expressions of $A^{(N)}$. After the expansion of Eq. (A1),

$$A_{m,n}^{(N)} \propto \beta_{mn}^{(N)} = \sum_{k=0}^{\infty} F_{mnk}(Ct)^k, \quad (\text{C6})$$

the main task is to identify the behavior of the series $\beta_{m,n}^{(N)}$, that is, the rule behind the terms F_{mnk} . Therefore, efficient computation of the amplitudes of the output modes requires knowing the convergence of the series expansion $\beta_{m,n}^{(N)}$ from the BCH formula for any N . This series expansion is related to several interesting problems in mathematics, as we will now discuss.

For $N \geq 5$, the coefficients in the series expansions are associated with less known successions. Table I presents the sequences appearing in the expansions of $\beta_{1,1}^{(N)}$ and $\beta_{N,N}^{(N)}$ for $N \leq 8$, identified by their respective OEIS codes [62]. For $N > 8$, we cannot unequivocally identify the sequences with the current OEIS database. We notice that the sequence expanding the entries of the evolution matrix $A^{(N)}$ of an N -mode system differs from those of an $(N-1)$ -mode system at the N th place (highlighted with italics in Table I). The sequences clearly show that the effect of adding a mode to a $(N-1)$ -mode system manifests at the N th order in the series expansion for the output operator. Such sequences can be found recursively for arbitrary $N > 2$ using their *generating function* $G_N(x)$, defined by $G_N(x) = 1/[1 - xG_{N-1}(x)]$, with $G_2(x) = 1/(1-x)$, show in Table I.

Finding the generating function $G_N(x)$ for all the matrix coefficients $\beta_{i,j}$ is more complicated, although it is still a feasible

approach to obtain the respective sequences. However, the effect of having arbitrary phases δ_i in the coupling coefficients requires a specific definition of G_N for each coefficient, so we must take a different approach for the present case.

2. General relations

For the open array [Fig. 1(b)], the complex entries of the transformation matrix $A^{(N)}$ can be generally expressed as

$$A_{m,n}^{(N)} = \exp(-i\phi_{m,n})\beta_{m,n}^{(N)}. \quad (\text{C7})$$

An evaluation of the recursive terms in Eq. (A2) leads to

$$\phi_{m,n} = \Delta_{m-1} - \Delta_{n-1}, \quad (\text{C8})$$

with $\Delta_n = \delta_1 + \delta_2 + \dots + \delta_n$. All of the information about the complex phases of the respective coupling coefficients is captured by $\phi_{m,n}$.

Such a simple expression for the phase $\phi_{m,n}$ is a unique feature of the open one-dimensional model. As discussed in Ref. [39], this and other particular geometries allow the unitary operation with complex coupling to be decomposed in three stages: evolution with real-valued coupling preceded and succeeded by individual phase shifts on each mode. In this geometry, the asymmetry introduced by the complex coupling coefficients is not expected to affect the transition probabilities from one mode to the other, but only the transition amplitudes.

For the closed N -mer [Fig. 1(c)], a factorization of the phase ϕ_{mn} analog to Eq. (C8) could not be found since the entries of $A^{(N)}$ behave differently from the open array. Considering equal phases $\delta_j = \delta$, the evaluation of Eq. (A2) leads to expressions of the form

$$\bar{A}_{1,n}^{(N)} = \sum_{l=1}^{\infty} \sigma_{N,n,l} \exp[(-1)^{l+1} b_l(N, n) \delta i] \beta_{nb_l}^{(N)}, \quad (\text{C9})$$

where $\sigma_{N,k,l}$ is the sign function; $b_l(N, n)$ are a set of integer numbers and $\beta_{nb_l}^{(N)}$ follows the definition in Eq. (C6).

As can be seen in Eq. (C9), the phase of the complex coupling coefficients is embedded in every term of the expansions. Although there is no factorization of the phases such as Eq. (C8) for the close N -mer, the only change with arbitrary phases is that δ become functions of all the phases, $\delta = \delta(\delta_1, \delta_2, \dots, \delta_N)$.

3. Successive method

As was pointed out in the case of $A_{1,2}^{(4)}$ [Eq. (C5)], F_{mnk} is linked to integer sequences. If the nature of these numerical successions is recursive, we can write them as

$$S_{n+r} = Q_1 S_{n+r-1} + Q_2 S_{n+r-2} + \dots + Q_r S_n, \quad (\text{C10})$$

where r is the recursive order and Q_r integer numbers (for instance, for the Fibonacci sequence $r = 2$ and $Q_1 = Q_2 = 1$). Equation (C10) can be cast into matrix form,

$$\mathbf{S}_j^{(N)} = R^{(N)} \mathbf{S}_{j-1}^{(N)}, \quad (\text{C11})$$

with $R^{(N)}$ the recursion matrix and $\mathbf{S}_j^{(N)}$ a vector composed of r successive terms in the sequence, i.e.,

$$\mathbf{S}_j^{(N)} = \begin{pmatrix} S_{j+r-1} \\ S_{j+r-2} \\ \vdots \\ S_j \end{pmatrix}, \quad (\text{C12})$$

$$R^{(N)} = \begin{pmatrix} Q_1 & Q_2 & \dots & Q_{r-1} & Q_r \\ 1 & 0 & \dots & 0 & 0 \\ 0 & 1 & \dots & 0 & 0 \\ \vdots & \vdots & \ddots & \vdots & \vdots \\ 0 & 0 & \dots & 1 & 0 \end{pmatrix}. \quad (\text{C13})$$

The superscript (N) is written to indicate the relationship to the transformation matrix $A^{(N)}$. Then Eq. (C11) can be rewritten by decomposing the initial condition $\mathbf{S}_0^{(N)}$ on the eigenvectors $\{\varphi_j\}$ of the recursion matrix $R^{(N)}$. This leads to the following expression for the j th term in the sequence:

$$S_j^{(N)} = \sum_{l=1}^r \eta_l \varphi_l^j, \quad (\text{C14})$$

where φ_l is the l th eigenvalue of $R^{(N)}$. In Eq. (C4), we have $\eta_1 = 1/\sqrt{5}$, $\eta_2 = -1/\sqrt{5}$, $\varphi_1 = (1 + \sqrt{5})/2$, and $\varphi_2 = (1 - \sqrt{5})/2$. The initial condition $\mathbf{S}_0^{(N)}$ is specific for each entry in the transformation matrix.

This formalism reduces the problem to diagonalize the recursion matrix $R^{(N)}$, i.e., to find the roots φ_l of its characteristic polynomial; afterwards, we must find the coefficients η_l in Eq. (C14).

The first task is addressed by different methods depending on the chosen framework. For the open tight-binding system [Eq. (C1)], in the geometrical study of *golden fields* it was found that diagonals of regular N -side polygons are proportional to the ratio of successive terms in generalized Fibonacci sequences [63]. This correspondence, described by the *diagonal product formula* (DPF), shows that characteristic polynomials can be expressed in terms of the Fibonacci polynomials of the second kind $K_n(x)$ [64], which, in turn, relate to the Chebyshev polynomials of the second kind $U_N(x)$ [64],

$$K_{N+1}(x) = U_N(x/2). \quad (\text{C15})$$

Chebyshev polynomials are a key element in our search for a general transformation matrix, inasmuch as is known that the roots of $U_N(x)$ are given by $x_k = \cos[k\pi/(N+1)]$ [65], for $k = 1, \dots, N$. Substituting in Eq. (C15), the roots of the $K_N(x)$ are obtained as

$$\varphi_k = 2 \cos\left(\frac{k\pi}{N+1}\right), \quad k = 1, \dots, N. \quad (\text{C16})$$

The above derivation not only gives the eigenvalues of the recursive matrix R , but also illustrates the relation between an N -mode lattice, the Fibonacci-like sequences, and the associated polynomial families.

To determine the η_l coefficients, it is essential to examine the initial condition \mathbf{S}_0 of the succession behind the F_{mnk} . The direct manner to come by them is to look at the first terms in

the expansion of Eq. (A1). This procedure must be carried out with caution since *a priori* r is not known or how many initial conditions exist. In the case $N = 6$, we found that $Q_1 = 1, Q_2 = 2, Q_3 = -1$ and three initial conditions,

$$\mathbf{S}_0^{(6)} = \begin{pmatrix} 2 \\ 0 \\ 1 \end{pmatrix}, \quad \begin{pmatrix} 1 \\ 0 \\ 0 \end{pmatrix}, \quad \begin{pmatrix} 2 \\ 1 \\ 1 \end{pmatrix}. \tag{C17}$$

From Eq. (C17), all the sequences to describe $A^{(6)}$ were determined, namely,

$$\begin{pmatrix} 2 \\ 0 \\ 1 \end{pmatrix} \rightarrow \{1, 0, 2, 1, 5, 5, 14, 19, 42, 66, 131, \dots\}, \tag{C18}$$

$$\begin{pmatrix} 1 \\ 0 \\ 0 \end{pmatrix} \rightarrow \{0, 0, 1, 1, 3, 4, 9, 14, 28, 47, 89, 155, \dots\}, \tag{C19}$$

$$\begin{pmatrix} 2 \\ 1 \\ 1 \end{pmatrix} \rightarrow \{1, 1, 2, 3, 6, 10, 19, 33, 61, 108, 197, \dots\}. \tag{C20}$$

Note that the expansion of Eq. (A1) by means of the BCH formula can always be done regardless of the complexity of the tight-binding interactions in the Hamiltonian. Notwithstanding, finding a formula to describe the integer sequences is not a straightforward task if no information about them is available in the OEIS. Given the recursive nature of the BCH formula, it is expected that the expansion of (A1) gives rise to recursive sequences. However, this is not always the case, as we will see in the close N -mer.

A more manageable scenery comes to light when we face the case of the closed array [Fig. 1(c)] because the sequences that appear are just binomial coefficients. For example, for $N = 5$, the entry $\bar{A}_{1,2}^{(5)}$ results in

$$\begin{aligned} \bar{A}_{1,2}^{(5)} = & e^{i(\delta-\pi/2)} \left[Ct - \frac{3}{3!}(Ct)^3 + \frac{10}{5!}(Ct)^5 - \frac{35}{7!}(Ct)^7 + \frac{126}{9!}(Ct)^9 - \frac{462}{11!}(Ct)^{11} + \frac{1716}{13!}(Ct)^{13} - \dots \right] \\ & + e^{-4i(\delta-\pi/2)} \left[\frac{(Ct)^4}{4!} - \frac{6}{6!}(Ct)^6 + \frac{28}{8!}(Ct)^8 - \frac{120}{10!}(Ct)^{10} + \frac{495}{12!}(Ct)^{12} - \frac{2002}{14!}(Ct)^{14} + \dots \right] \\ & + e^{6i(\delta-\pi/2)} \left[\frac{(Ct)^6}{6!} - \frac{8}{8!}(Ct)^8 + \frac{45}{10!}(Ct)^{10} - \frac{220}{12!}(Ct)^{12} + \frac{1001}{14!}(Ct)^{14} - \frac{4368}{16!}(Ct)^{16} + \dots \right] \\ & + e^{-9i(\delta-\pi/2)} \left[-\frac{(Ct)^9}{9!} + \frac{11}{11!}(Ct)^{11} - \frac{78}{13!}(Ct)^{13} + \frac{445}{15!}(Ct)^{15} - \frac{2380}{17!}(Ct)^{17} + \frac{11628}{19!}(Ct)^{19} - \dots \right] \\ & + e^{11i(\delta-\pi/2)} \left[\frac{(Ct)^{11}}{11!} - \frac{13}{13!}(Ct)^{13} + \frac{105}{15!}(Ct)^{15} - \frac{680}{17!}(Ct)^{17} + \frac{3876}{19!}(Ct)^{19} - \frac{20349}{21!}(Ct)^{21} + \dots \right] \\ & + e^{-14i(\delta-\pi/2)} \left[\frac{(Ct)^{14}}{14!} - \frac{16}{16!}(Ct)^{16} + \frac{153}{18!}(Ct)^{18} - \frac{1140}{20!}(Ct)^{20} + \frac{7315}{22!}(Ct)^{22} - \frac{42504}{24!}(Ct)^{24} + \dots \right] \\ & + e^{16i(\delta-\pi/2)} \left[\frac{(Ct)^{16}}{16!} - \frac{18}{18!}(Ct)^{18} + \frac{190}{20!}(Ct)^{20} - \frac{1540}{22!}(Ct)^{22} + \frac{10626}{24!}(Ct)^{24} - \frac{65780}{26!}(Ct)^{26} + \dots \right] \\ & + e^{-19i(\delta-\pi/2)} \left[-\frac{(Ct)^{19}}{19!} + \frac{21}{21!}(Ct)^{21} - \frac{253}{23!}(Ct)^{23} + \frac{2300}{25!}(Ct)^{25} - \frac{17550}{27!}(Ct)^{27} + \frac{118755}{29!}(Ct)^{29} - \dots \right] + \dots \end{aligned} \tag{C21}$$

The coefficients in the series given by Eq. (C21) with factor $e^{i(\delta-\pi/2)}$ were identified to be

$$1, 3, 10, 35, 126, 462, 1716, \dots \rightarrow \binom{2n+1}{n+1}. \quad (C22)$$

With these coefficients, we were able to converge this series, obtaining

$$\begin{aligned} \beta_{2,1}^{(5)} &= \sum_{n=0}^{\infty} \binom{2n+1}{n+1} \frac{(-1)^n}{(2n+1)!} (Ct)^{2n+1}, \\ \beta_{2,1}^{(5)} &= \sum_{n=0}^{\infty} \frac{(2n+1)!}{(n+1)!n!} \frac{(-1)^n}{(2n+1)!} (Ct)^{2n+1}, \\ \beta_{2,1}^{(5)} &= \sum_{n=0}^{\infty} \frac{(-1)^n}{n!(n+1)!} (Ct)^{2n+1}, \\ \beta_{2,1}^{(5)} &= J_1(2Ct). \end{aligned} \quad (C23)$$

Following the same procedure for the remaining complex exponentials, the $\beta_{2,b_l}^{(5)}$ factors were also turned to be Bessel functions of the first kind whose indexes were b_l . This is summarized as follows:

$$\beta_{nb_l}^{(N)} = J_{b_l}(2Ct), \quad (C24)$$

$$b_l(5, 2) = \{1, 4, 6, 9, 11, 14, 16, 19, \dots\}. \quad (C25)$$

Replacing the series in Eq. (C21) by their respective Bessel functions results in

$$\begin{aligned} \bar{A}_{1,2}^{(5)} &= e^{i(\delta-\pi/2)} J_1(2Ct) + e^{-4i(\delta-\pi/2)} J_4(2Ct) \\ &+ e^{6i(\delta-\pi/2)} J_6(2Ct) - e^{-9i(\delta-\pi/2)} J_9(2Ct) \\ &+ e^{11i(\delta-\pi/2)} J_{11}(2Ct) + e^{-14i(\delta-\pi/2)} J_{14}(2Ct) \\ &+ e^{16i(\delta-\pi/2)} J_{16}(2Ct) - e^{-19i(\delta-\pi/2)} J_{19}(2Ct) + \dots \end{aligned} \quad (C26)$$

The alternating minus sign over the terms of the series given by Eq. (C26) does not follow a pattern $(-1)^k$ like the minus sign over the argument of the complex exponentials. The rule for this minus sign is captured by the $\sigma_{N,n,l}$ function defined in Eq. (C30). Following the same strategy, all the entries of $\bar{A}^{(N)}$ were found, obtaining

$$\bar{A}_{1,n}^{(N)} = \begin{cases} \alpha_N^{(1)}, & N \text{ odd}, \quad n = 1 \\ \alpha_{N,n}^{(2)}, & N \text{ odd}, \quad n \leq (N+1)/2 \\ \mathcal{P}_c \alpha_{N,N-n+2}^{(2)}, & N \text{ odd}, \quad n > (N+1)/2 \\ \alpha_N^{(0)}, & N \text{ even}, \quad n = 1 \\ \alpha_{N,n}^{(2)}, & N \text{ even}, \quad n \leq N/2 \\ \alpha_{N,n}^{(3)}, & N \text{ even}, \quad n = \frac{N}{2} + 1, \quad n \text{ odd} \\ \alpha_{N,n}^{(4)}, & N \text{ even}, \quad n = \frac{N}{2} + 1, \quad n \text{ even} \\ \alpha_{N,N-n+2}^{(2)*}, & N \text{ even}, \quad n > \frac{N}{2} + 1, \quad n \text{ odd} \\ -\alpha_{N,N-n+2}^{(2)*}, & N \text{ even}, \quad n > \frac{N}{2} + 1, \quad n \text{ even}, \end{cases} \quad (C27)$$

where the $\alpha_{N,n}$ functions are given by

$$\begin{aligned} \alpha_N^{(0)} &= -J_0(2Ct) + 2 \sum_{l=0}^{\infty} \cos [lN(\delta - \pi/2)] J_{lN}(2Ct), \\ \alpha_N^{(1)} &= -J_0(2Ct) \\ &+ 2 \sum_{l=0}^{\infty} \{ \cos [2lN(\delta - \pi/2)] J_{2lN}(2Ct) \\ &+ i \sin [(2l+1)N(\delta - \pi/2)] J_{(2l+1)N}(2Ct) \}, \\ \alpha_{N,n}^{(2)} &= \sum_{l=1}^{\infty} \sigma_{N,n,l} \exp [(-1)^{l+1} b_l(N, n)(\delta - \pi/2)i] \\ &\times J_{b_l}(2Ct), \\ \alpha_{N,n}^{(3)} &= 2 \sum_{l=0}^{\infty} \cos \left[\frac{N}{2} (2l+1)(\delta - \pi/2) \right] J_{N(2l+1)/2}(2Ct), \\ \alpha_{N,n}^{(4)} &= 2i \sum_{l=0}^{\infty} \sin \left[\frac{N}{2} (2l+1)(\delta - \pi/2) \right] J_{N(2l+1)/2}(2Ct), \end{aligned} \quad (C28)$$

with indexes $b_l(N, n)$ defined by the set

$$b_l(N, n) = \{k \in \mathbb{N} \mid k = n - 1 \vee N - n + 1 \pmod{N}\}, \quad (C29)$$

and the special sign function

$$\sigma_{N,n,l} = \begin{cases} \sigma_1[b_l(N, n)], & N \text{ odd}, \quad n \text{ even} \\ \sigma_2[b_l(N, n)], & N \text{ odd}, \quad n \text{ odd} \\ (-1)^{l+1}, & N \text{ even}, \quad n \text{ even} \\ 1, & N \text{ even}, \quad n \text{ odd}, \end{cases}$$

$$\sigma_1[b_l(N, n)] = \begin{cases} -1, & b_l(N, n) = 2N - n + 1 \pmod{2N} \\ 1 & \text{otherwise}, \end{cases}$$

$$\sigma_2[b_l(N, n)] = \begin{cases} -1, & b_l(N, n) = N - n + 1 \pmod{N} \\ 1 & \text{otherwise}, \end{cases}, \quad (C30)$$

with a parity conjugation operator

$$\mathcal{P}_c e^{in\delta} = \begin{cases} -e^{-in\delta}, & n \text{ odd} \\ e^{-in\delta}, & n \text{ even}. \end{cases} \quad (C31)$$

The $\alpha_{N,n}$ functions for the entries of $A^{(N)}$ resemble the Jacobi-Anger expansions, but with a major detail on the indexes of the series. This feature make us unable to converge the series in Eq. (C28). It is important to highlight the versatility of the previous formalism since Eqs. (C7) and (C14) hold for any set of coupling coefficients, in addition to the two one-dimensional cases studied here. This allows us to extend our study to any two-dimensional system that can be mapped to a one-dimensional matrix, provided that the appropriate integer sequence (or its recurrence matrix) is known.

4. Path method

Coefficients η_j in Eq. (C14) are still required to find the sequence describing the entries of the transformation matrix. However, we can use the link between quantum random walks

and graph theory, provided by the aforementioned equivalence between the coupling matrix \mathcal{C} (corresponding to the single-particle representation of H) and the adjacency matrix \mathcal{J} of the associated path graph P_N . If G is a graph with weights at the edges and adjacency matrix $\mathcal{J}_{N,\varrho}$, where N is the number of vertices and ϱ is the weight of the loops, then the sum of weights of walks of length m from vertex i to j is given by $(e_i^T)(\mathcal{J}_{N,\varrho}^m)(e_j)$. Defining $Z_{i,j}^N(m, \ell)$ as the number of walks from i to j of length m , and using ℓ loops in P_n , the following can be obtained [42]:

$$\sum_{\ell=0}^m Z_{i,j}^N(m, \ell)\varrho^\ell = (e_i^T)(\mathcal{J}_{N,\varrho}^m)(e_j). \quad (C32)$$

This is precisely the expression we need in order to write Eq. (A10) more effectively. Obtaining an expression for the left-hand side of Eq. (C32) is straightforward when considering the spectrum of the adjacency matrix. If $\mathcal{J}_{N,\varrho}$ admits an orthonormal basis (v_1, v_2, \dots, v_N) of eigenvectors and $\lambda_i \in \mathbb{C}$ is the eigenvalue corresponding to $v_i = (v_{1,i}, v_{2,i}, \dots, v_{N,i})$, then

$$(e_i^T)(\mathcal{J}_{N,\varrho}^m)(e_j) = \sum_{k=1}^N \lambda_k^m v_{i,k} v_{j,k}. \quad (C33)$$

In the particular case of $\mathcal{J}_{N,0}$ the eigenvalues λ_k and eigenvectors v_k are given by

$$\lambda_k = 2 \cos\left(\frac{k\pi}{N+1}\right) \quad (C34)$$

and

$$v_k = \left[\sin\left(1 \times \frac{k\pi}{N+1}\right), \sin\left(2 \times \frac{k\pi}{N+1}\right), \dots, N \times \sin\left(\frac{k\pi}{N+1}\right) \right], \quad (C35)$$

for $k = 1, 2, \dots, N$. Note that Eq. (C34) is identical to the expression obtained in Eq. (C16). This illustrates a close relationship between the Chebyshev polynomials of the second kind and their roots and eigenvalues of the adjacency matrix displayed above. Replacing Eqs. (C34) and (C35) in Eq. (C33) and using Eq. (C32) enables us to obtain an explicit expression for the numbers $Z_{i,j}^N(m, \ell)$ in terms of trigonometric sums. Assuming $\ell = 0$, in the case where we have open arrays, the $Z_{i,j}^N(m)$ numbers are given by

$$Z_{i,j}^{(N_{\text{open}})}(m) = \frac{2}{N+1} \sum_{k=1}^N \left[2 \cos\left(\frac{k\pi}{N+1}\right) \right]^m \times \sin\left(\frac{ik\pi}{N+1}\right) \sin\left(\frac{jk\pi}{N+1}\right), \quad (C36)$$

for an N -mode open array with first-neighbor coupling, and for cycle graphs C_n , which correspond to paths where the walk begins at vertex i and ends at vertex j and which we associate with closed arrays, the numbers are given by

$$Z_{i,j}^{(N_{\text{closed}})}(m) = \frac{1}{n} \sum_{k=0}^{n-1} \left[2 \cos\left(k \frac{2\pi}{n}\right) \right]^m \cos\left(k \frac{2\pi(i-j)}{n}\right), \quad n = \begin{cases} N, & N \text{ even} \\ 2N, & N \text{ odd.} \end{cases} \quad (C37)$$

Equations (C14) and (C36) show the formal correspondence between the m th term in the series expansion of $A_{i,j}^{(N)}$ and the total number of all m -step paths, i.e., the path length corresponds to the order of the terms in the approximation given by Eq. (C7). This enables a straightforward physical interpretation of the path count: while adding $Z_{i,j}^{(N)}(m)$ for $0 < m < \infty$ would give the number of all possible paths between vertices i and j , $A_{i,j}^{(N)}$, on the other hand, captures the superposition of all the contributions, resulting in the excitation of waveguide a_i by an initial excitation of waveguide a_j . Indeed, the Z numbers can be considered a universal quantity, and terms in many numerical successions, including the Fibonacci and Catalan sequences, can be obtained as particular cases of them [42].

In order to construct the complete entry $A_{\mu,\nu}^{(N)}$, we must sum the number $Z_{i,j}^{(N)}(m)$ defined in Eq. (C36) over all the path lengths m from 0 to ∞ . Also, we need to modify the sum in the equation to take into account the complex phases δ_i present in the coupling coefficients Λ_i . By doing so, we finally obtain

$$A_{\mu,\nu}^{(N)} = \frac{2}{N+1} \sum_{k=1}^N \exp\left[-2i \cos\left(\frac{k\pi}{N+1}\right) Ct\right] S_{\mu\nu k}, \quad (C38)$$

where

$$S_{\mu\nu k} = \exp\left\{-i\left[\frac{\pi}{2}(\mu - \nu) + \Delta_{\mu-1} - \Delta_{\nu-1}\right]\right\} \times \sin\left(\frac{\mu k\pi}{N+1}\right) \sin\left(\frac{\nu k\pi}{N+1}\right), \quad (C39)$$

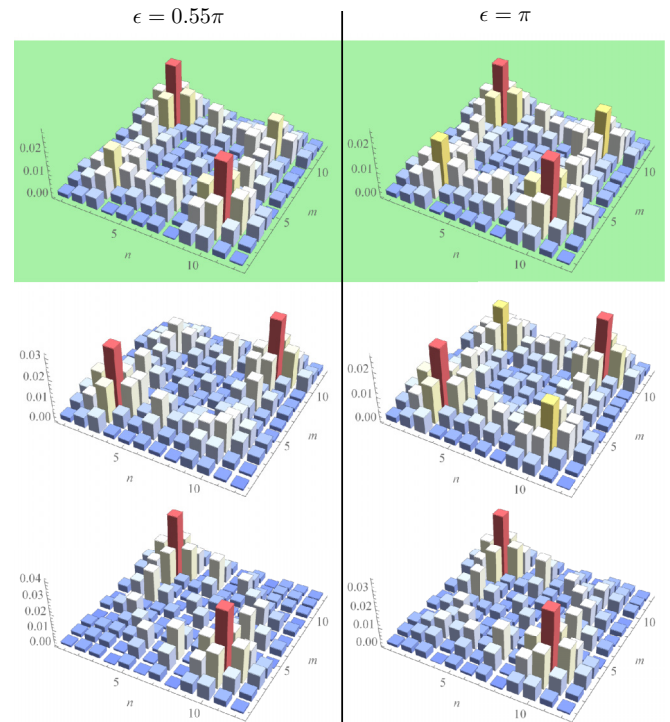


FIG. 8. Representative examples of the different correlation profiles obtained from individual realizations when disorder is present in the complex phases of the coupling coefficients.

and the terms $\Delta_\nu = \delta_1 + \delta_2 + \dots + \delta_\nu$ contain the information about the phases of the coupling coefficients $C_j = C \exp(i\delta_j)$, with C being their real amplitude. On the other hand, the *closed* system, i.e., the N -mer where the first and the N th modes are also coupled, is described by a transformation matrix $\bar{A}^{(N)}$, whose n th row is obtained by *cycling* n times the first row with entries

$$\bar{A}_{1,n}^{(N)} = \frac{e^{2iCt}}{N} + \frac{2}{N} \sum_{k=1}^{(N-1)/2} (-1)^{(n-1)k} \cos \left[(n-1)k \frac{\pi}{N} \right] \times \exp \left[(-1)^k 2iCt \cos \left(k \frac{\pi}{N} \right) \right], \quad (\text{C40})$$

for N odd. For N even, its elements are given by

$$\bar{A}_{1,n}^{(N)} = \frac{1}{N} \sum_{k=0}^{N-1} \cos \left[(n-1)k \frac{2\pi}{N} \right] \times \begin{cases} \cos \left[2Ct \cos \left(k \frac{2\pi}{N} \right) \right], & n \text{ odd} \\ i \sin \left[2Ct \cos \left(k \frac{2\pi}{N} \right) \right], & n \text{ even.} \end{cases} \quad (\text{C41})$$

APPENDIX D: EXAMPLES OF CORRELATION PROFILES FOR INDIVIDUAL REALIZATIONS

In Sec. III D, we presented the analytic average correlation patterns obtained for different degrees of decoherence ϵ . Here we present some illustrative profiles of single realizations corresponding to random choices for the coefficients phases with a normal width distribution ϵ . These provide examples of different outputs occurring with different frequencies, resulting in the average profiles presented in the main text. Note that the effects of having disorder in the phases of the coupling coefficients clearly differ from the well-studied off-diagonal disorder in the amplitudes of the coefficients, which is known to induce Anderson localization. In our case, no localization is observed. Instead, the effect of phase disorder shows in the interference. In Fig. 8, the highlighted profile for each case resembles the most frequent outputs in a qualitative review of the individual realizations. The first example is the most representative for $\epsilon = 0.55\pi$ (left column); bunching and antibunching still occur, with the latter being more probable. On the other hand, for $\epsilon = \pi$ (right column), most cases lead to a four-peak profile in the output, with bunching and antibunching still occasionally occurring.

-
- [1] N. W. Ashcroft and N. D. Mermin, *Solid State Physics* (Thomson Learning, Toronto, London, 1976).
- [2] I. Bloch, J. Dalibard, and W. Zwerger, Many-body physics with ultracold gases, *Rev. Mod. Phys.* **80**, 885 (2008).
- [3] M. Lewenstein, A. Sanpera, V. Ahufinger, and B. Damski, Ultracold atomic gases in optical lattices: Mimicking condensed matter physics and beyond, *Adv. Phys.* **56**, 243 (2007).
- [4] M. Segev, Y. Silberberg, and D. N. Christodoulides, Anderson localization of light, *Nat. Photon.* **7**, 197 (2013).
- [5] A. Szameit and S. Nolte, Discrete optics in femtosecond-laser-written photonic structures, *J. Phys. B: At. Mol. Opt. Phys.* **43**, 163001 (2010).
- [6] S. Longhi, Quantum-optical analogies using photonic structures, *Laser Photon. Rev.* **3**, 243 (2009).
- [7] Y. Chen, X. Chen, X. Ren, M. Gong, and G.-c. Guo, Tight-binding model in optical waveguides: Design principle and transferability for simulation of complex photonics networks, *Phys. Rev. A* **104**, 023501 (2021).
- [8] F. Lederer, G. I. Stegeman, D. N. Christodoulides, G. Assanto, M. Segev, and Y. Silberberg, Discrete solitons in optics, *Phys. Rep.* **463**, 1 (2008).
- [9] M. Mattarelli, M. Secchi, and M. Montagna, Phononic crystals of spherical particles: A tight binding approach, *J. Chem. Phys.* **139**, 174710 (2013).
- [10] K.-I. Imura, M. Okamoto, Y. Yoshimura, Y. Takane, and T. Ohtsuki, Finite-size energy gap in weak and strong topological insulators, *Phys. Rev. B* **86**, 245436 (2012).
- [11] J. Medina Dueñas, G. O’Ryan Pérez, C. Hermann-Avigliano, and L. E. F. Foa Torres, Quadrature protection of squeezed states in a one-dimensional photonic topological insulator, *Quantum* **5**, 526 (2021).
- [12] G. O’Ryan Pérez, J. Medina Dueñas, D. Guzmán-Silva, L. E. F. Foa Torres, and C. Hermann-Avigliano, Transport of non-classical light mediated by topological domain walls in a SSH photonic lattice, *Sci. Rep.* **14**, 12435 (2024).
- [13] Y. Bromberg, Y. Lahini, R. Morandotti, and Y. Silberberg, Quantum and classical correlations in waveguide lattices, *Phys. Rev. Lett.* **102**, 253904 (2009).
- [14] A. Peruzzo, M. Lobino, J. C. F. Matthews, N. Matsuda, A. Politi, K. Poulios, X.-Q. Zhou, Y. Lahini, N. Ismail, K. Wörhoff, Y. Bromberg, Y. Silberberg, M. G. Thompson, and J. L. O’Brien, Quantum walks of correlated photons, *Science* **329**, 1500 (2010).
- [15] J. M. Zhang and R. X. Dong, Exact diagonalization: The Bose-Hubbard model as an example, *Eur. J. Phys.* **31**, 591 (2010).
- [16] A. W. Harrow, A. Hassidim, and S. Lloyd, Quantum algorithm for linear systems of equations, *Phys. Rev. Lett.* **103**, 150502 (2009).
- [17] S. Rojas-Rojas, E. Barriga, C. Muñoz, P. Solano, and C. Hermann-Avigliano, Manipulation of multimode squeezing in a coupled waveguide array, *Phys. Rev. A* **100**, 023841 (2019).
- [18] J. Wang, F. Sciarrino, A. Laing, and M. G. Thompson, Integrated photonic quantum technologies, *Nat. Photon.* **14**, 273 (2020).
- [19] A. Karimi, Two-mode photon-added entangled coherent-squeezed states: Their entanglement and nonclassical properties, *Appl. Phys. B* **123**, 181 (2017).
- [20] T. Q. Dat and T. M. Duc, Nonclassical properties of the superposition of three-mode photon-added trio coherent state, *Intl. J. Theor. Phys.* **59**, 3206 (2020).
- [21] Y. Yang, Enhancing quantum entanglement by combinations of photon additions and photon subtractions, *J. Opt. Soc. Am. B* **33**, 2545 (2016).
- [22] M. Walschaers, C. Fabre, V. Parigi, and N. Treps, Statistical signatures of multimode single-photon-added and -subtracted states of light, *Phys. Rev. A* **96**, 053835 (2017).

- [23] H. Zhang, W. Ye, S. Chang, Y. Xia, L. Hu, and Z. Liao, Quantum multiparameter estimation with multimode photon catalysis entangled squeezed state, *Front. Phys.* **18**, 42304 (2023).
- [24] J.-D. Zhang, Z.-J. Zhang, L.-Z. Cen, J.-Y. Hu, and Y. Zhao, Simultaneously estimating two phase shifts with a power-recycled tri-port interferometer fed by coherent states, *OSA Contin.* **1**, 1437 (2018).
- [25] D. Braun, P. Jian, O. Pinel, and N. Treps, Precision measurements with photon-subtracted or photon-added Gaussian states, *Phys. Rev. A* **90**, 013821 (2014).
- [26] O. S. Magaña-Loaiza, R. de J. León-Montiel, A. Perez-Leija, A. B. U'Ren, C. You, K. Busch, A. E. Lita, S. W. Nam, R. P. Mirin, and T. Gerrits, Multiphoton quantum-state engineering using conditional measurements, *npj Quantum Inf.* **5**, 80 (2019).
- [27] C. M. Bender, S. F. Brandt, J.-H. Chen, and Q. Wang, Ghost busting: Pt-symmetric interpretation of the Lee model, *Phys. Rev. D* **71**, 025014 (2005).
- [28] W.-P. Huang and J. Mu, Complex coupled-mode theory for optical waveguides, *Opt. Express* **17**, 19134 (2009).
- [29] Y. Aharonov, L. Davidovich, and N. Zagury, Quantum random walks, *Phys. Rev. A* **48**, 1687 (1993).
- [30] E. Nicolau, A. M. Marques, R. G. Dias, J. Mompert, and V. Ahufinger, Many-body Aharonov-Bohm caging in a lattice of rings, *Phys. Rev. A* **107**, 023305 (2023).
- [31] M. C. Rechtsman, J. M. Zeuner, Y. Plotnik, Y. Lumer, D. Podolsky, F. Dreisow, S. Nolte, M. Segev, and A. Szameit, Photonic Floquet topological insulators, *Nature (London)* **496**, 196 (2013).
- [32] B. A. Bell, K. Wang, A. S. Solntsev, D. N. Neshev, A. A. Sukhorukov, and B. J. Eggleton, Spectral photonic lattices with complex long-range coupling, *Optica* **4**, 1433 (2017).
- [33] S. Longhi, Non-Hermitian tight-binding network engineering, *Phys. Rev. A* **93**, 022102 (2016).
- [34] M. Walschaers, C. Fabre, V. Parigi, and N. Treps, Entanglement and Wigner function negativity of multimode non-Gaussian states, *Phys. Rev. Lett.* **119**, 183601 (2017).
- [35] A. Rai, G. S. Agarwal, and J. H. H. Perk, Transport and quantum walk of nonclassical light in coupled waveguides, *Phys. Rev. A* **78**, 042304 (2008).
- [36] A. Rostami and A. Javadi, *Nonclassical light in array of single mode optical waveguides*, in *Asia Communications and Photonics Conference and Exhibition (IEEE, Shanghai, China, 2010)*, pp. 212–213.
- [37] B. M. Rodríguez-Lara, Propagation of nonclassical states of light through one-dimensional photonic lattices, *J. Opt. Soc. Am. B* **31**, 878 (2014).
- [38] M. Dairyko, L. Padwell, S. Tyner, and C. Wynn, Noncontiguous pattern avoidance in binary trees, *Electron. J. Combinator.* **19**, P22 (2012).
- [39] D. Lu, J. D. Biamonte, J. Li, H. Li, T. H. Johnson, V. Bergholm, M. Faccin, Z. Zimborás, R. Laflamme, J. Baugh, and S. Lloyd, Chiral quantum walks, *Phys. Rev. A* **93**, 042302 (2016).
- [40] Z. Zimborás, M. Faccin, Z. Kádár, J. D. Whitfield, B. P. Lanyon, and J. Biamonte, Quantum transport enhancement by time-reversal symmetry breaking, *Sci. Rep.* **3**, 2361 (2013).
- [41] A. Sett, H. Pan, P. E. Falloon, and J. B. Wang, Zero transfer in continuous-time quantum walks, *Quantum Inf. Proc.* **18**, 159 (2019).
- [42] S. Felsner and D. Heldt, Lattice path enumeration and Toeplitz matrices, *J. Integer Seq.* **18**, 15.1.3 (2015).
- [43] Y. Liu and D. L. Zhou, Quantum state transfer along a ring with time-reversal asymmetry, *Phys. Rev. A* **91**, 052318 (2015).
- [44] L. Morales-Inostroza and R. A. Vicencio, Simple method to construct flat-band lattices, *Phys. Rev. A* **94**, 043831 (2016).
- [45] S. Rojas-Rojas, L. Morales-Inostroza, R. A. Vicencio, and A. Delgado, Quantum localized states in photonic flat-band lattices, *Phys. Rev. A* **96**, 043803 (2017).
- [46] A. Zavatta, S. Viciani, and M. Bellini, Quantum-to-classical transition with single-photon-added coherent states of light, *Science* **306**, 660 (2004).
- [47] N. T. X. Hoai and T. M. Duc, Nonclassical properties and teleportation in the two-mode photon-added displaced squeezed states, *Intl. J. Mod. Phys. B* **30**, 1650032 (2016).
- [48] R. Carranza and C. C. Gerry, Photon-subtracted two-mode squeezed vacuum states and applications to quantum optical interferometry, *J. Opt. Soc. Am. B* **29**, 2581 (2012).
- [49] R. de J. León-Montiel, O. S. Magaña-Loaiza, A. Perez-Leija, A. U'ren, K. Busch, A. E. Lita, S. W. Nam, T. Gerrits, and R. P. Mirin, *Generation of photon-subtracted two-mode squeezed vacuum states*, in *Frontiers in Optics / Laser Science* (Optica Publishing Group, 2018), pp. LM1B.6.
- [50] A. Dufour, C. Jacquard, Y.-S. Ra, C. Fabre, and N. Treps, *Photon subtraction from a multimode squeezed vacuum state*, in *Quantum Information and Measurement (QIM) 2017* (Optica Publishing Group, 2017), pp. QT4B.2.
- [51] T. Q. Dat, and T. M. Duc, Higher-order nonclassical and entanglement properties in photon-added trio coherent state, *Hue Univ. J. Science: Nat. Sci.* **129**, 49 (2020).
- [52] G. Yeoman and S. M. Barnett, Two-mode squeezed Gaussons, *J. Mod. Opt.* **40**, 1497 (1993).
- [53] S. Braunstein and P. van Loock, Quantum information with continuous variables, *Rev. Mod. Phys.* **77**, 513 (2005).
- [54] A. Kenfack and K. Życzkowski, Negativity of the Wigner function as an indicator of nonclassicality, *J. Opt. B: Quantum Semiclass. Opt.* **6**, 396 (2004).
- [55] F. Siyouri, M. El Baz, and Y. Hassouni, The negativity of Wigner function as a measure of quantum correlations, *Quantum Inf. Proc.* **15**, 4237 (2016).
- [56] M. Uria, P. Solano, and C. Hermann-Avigliano, Deterministic generation of large Fock states, *Phys. Rev. Lett.* **125**, 093603 (2020).
- [57] M. Uria, A. Maldonado-Trapp, C. Hermann-Avigliano, and P. Solano, Emergence of non-Gaussian coherent states through nonlinear interactions, *Phys. Rev. Res.* **5**, 013165 (2023).
- [58] O. Pinel, J. Fade, D. Braun, P. Jian, N. Treps, and C. Fabre, Ultimate sensitivity of precision measurements with intense Gaussian quantum light: A multimodal approach, *Phys. Rev. A* **85**, 010101(R) (2012).
- [59] K. V. Kheruntsyan, J.-C. Jaskula, P. Deuar, M. Bonneau, G. B. Partridge, J. Ruaudel, R. Lopes, D. Boiron, and C. I. Westbrook, Violation of the Cauchy-Schwarz inequality with matter waves, *Phys. Rev. Lett.* **108**, 260401 (2012).

- [60] J. R. Johansson, P. D. Nation, and F. Nori, QuTip: An open-source Python framework for the dynamics of open quantum systems, *Comput. Phys. Commun.* **183**, 1760 (2012).
- [61] W. R. Spickerman, Binet's formula for the tribonacci sequence, *Fibonacci Quart.* **20**, 118 (1982).
- [62] OEIS Foundation Inc., The on-line encyclopedia of integer sequences (2022), <http://oeis.org>.
- [63] P. Steinbach, Golden fields: A case for the heptagon, *Math. Mag.* **70**, 22 (1997).
- [64] J. Kappraff, S. Jablan, G. W. Adamson, and R. Sazdanovich, Golden fields, generalized Fibonacci sequences, and chaotic matrices, *Forma* **19**, 367 (2004).
- [65] J. C. Mason and D. C. Handscomb, *Chebyshev Polynomials* (CRC Press, Boca Raton, FL, 2002).